Application of LQR and H_2-optimal Control for a Quadrotor System

by

Chen Ma

B.Sc., Hangzhou University, 1995

M.Eng., Huazhong University of Science and Technology, 2009

A Thesis Submitted in Partial Fulfillment of the

Requirements for the Degree of

MASTER OF APPLIED SCIENCE

in the Department of Mechanical Engineering

Application of LQR and H_2-optimal Control for a Quadrotor System

by

Chen Ma

B.Sc., Hangzhou University, 1995

M.Eng., Huazhong University of Science and Technology, 2009

Supervisory Committee

Dr. Yang Shi, Supervisor

(Department of Mechanical Engineering)

Dr. Ben Nadler, Committee Member

(Department of Mechanical Engineering)

Supervisory Committee

Dr. Yang Shi, Supervisor

(Department of Mechanical Engineering)

Dr. Ben Nadler, Committee Member

(Department of Mechanical Engineering)

ABSTRACT

A quadrotor is a type of small unmanned aerial vehicle (UAV) with four rotors. Various control techniques have been successfully applied to the quadrotor. In this thesis, two control methods, including linear quadratic regulator (LQR) and H_2-optimal control, are applied to the autonomous navigation and control of a quadorotor named QBall-X4 that is developed by Quanser.

The continuous-time dynamic model is established using the Euler-Lagrange approach. Due to the nonlinearities in the quadrotor dynamics, we propose a simplified linear model, which is further used for the controller design in this thesis.

According to the simplified quadrotor dynamics, we design an LQR controller to regulate the quadrotor system from its initial position to the desired position. The effectiveness of the controller is verified by simulation studies. However, the LQR control system is operated in the nominal model, and it can not present guaranteed performance when system uncertainties exist.

The main emphasis is placed on designing an H_2-optimal controller that minimizes the H_2-norm of the transfer function. The solution is obtained by using the state-space approach and linear matrix inequality (LMI) method, respectively. In contrast to LQR control method, which is normally applied to a system with no disturbance, the H_2-optimal controller takes the form of an observer together with a state feedback control gain to deal with the system uncertainties and disturbances. The simulation results and experimental study verify that the proposed H_2-optimal controller is an effective option for the quadrotor with the attendance of uncertainties and disturbances.

Table of Contents

List of Figures

Acknowledgements

First, I would like to thank my supervisor, Prof. Yang Shi. I appreciate his valuable suggestions regarding the opportunity to study in Canada, the patient guidance for my research topics, the ample encouragement he has provided throughout my work, and the understanding of my responsibility for my family. I am so grateful to have a supervisor who can be a role model in my life.

Moreover, I would like to thank all of the group members. Thank Huaiyuan Sheng for helping me to review all of the related theoretical basis and taking the time to revise my thesis. Thank Kunwu Zhang and Changxin Liu for their suggestions to derive the mathematical equations and the control algorithms. Thank Dr. Bingxian Mu for the introduction of the experimental system. Thank Xinxin Shang and Qi Sun for their kindly reminder emails. Thank Yuan Yang for sharing me his creative thinking. My sincere thanks also go to the group members, for their efforts put to revise the draft of my thesis. I feel so fortunate to be a part of this wonderful group.

Next, I want to take a moment to express my gratitude to my husband, Huxiong Li. Without his encouragement, I can not return to school and study on my favorite major, especially I have been out of the classroom for a long time. Thanks for his love, financial support, and patience throughout the difficult time.

Finally, but most importantly, I would like to thank my parents, my sister, and my son, for their selfless love and support. I love them all.

Chen Ma

Acronyms

UAV unmanned aerial vehicle

LQR linear quadratic regulator

LMI linear matrix inequality

PID proportional-integral-derivative

MPC model predictive control

LQG linear quadratic Gaussian

LTI linear time-invariant

LAN local area network

COG the center of gravity

DOF degrees of freedom

PWM pulse width modulation

LQE linear quadratic estimator

Chapter 1

Introduction

1.1 Brief Introduction of Unmanned Aerial Vehicles

Unmanned aerial vehicles (UAVs) are a class of aircrafts which can fly without a human pilot on board. Over the last few decades, UAVs have been widely applied in military and civil areas. One example of the applications in military area is that UAVs are used in U.S. air strikes in Yemen and Somalia [3]. On the civil side, the applications include the traffic surveillance [4], photogrammetric recording [5], wildfire suppression [6], crops spraying [7], etc.

The UAVs are commonly classified by the size, configurations, range, and endurance. For example, based on their size, UAVs are classified as: micro small UAVs, small UAVs, medium UAVs, and large UAVs [8]. Based on configurations, UAVs can be classified as fixed-wing UAVs and rotary-wing UAVs [9]. Figure 1.1 shows a fixed-wing UAV, RQ-7B Shadow UAV, which is operated by U.S. Army, whereas Figure 1.2 shows a rotary-wing UAV applied in the agriculture sector. Compared to fixed-wing UAVs, the rotary-wing UAV has the capability of vertical take-off and

landing and better maneuverability [10]. Based on the number of rotors, rotary-wing UAVs are further classified as helicopters, quadrotors, hexrotors, and octorotors, etc.

Figure 1.1: RQ-7B Shadow UAV [1].

Figure 1.2: A UAV for farming [2].

1.2 Quadrotor Dynamic Model

As shown in Figure 1.3, the quadrotor has four propellers which are actuated by electric motors. One pair of propellers (propellers 2 and 4) rotate clockwise, while the other pair of propellers (propellers 1 and 3) rotate counterclockwise. When a propeller is rotating, it generates a thrust force and a reaction torque. The thrusts generated by all propellers have the same direction. The thrusts are denoted by f_1, f_2, f_3, f_4, and the reaction torques are denoted by τ_1, τ_2, τ_3, τ_4. For each propeller, the generated thrust force and reaction torque are proportional to the square of rotational speed of the propeller [11].

The motion of the quadrotor relates to the rotational speed of each of propeller. Figure 1.4 shows how the forces and torques generated by the rotational propellers affect the change of motions. For the motion in X-direction, the rotational speed of propeller 3 increases, and the rotational speed of propeller 1 decreases with the same value, producing a motion along X-direction. Similarly, the movement along Y-

[1] https://olive-drab.com/idphoto/id_photos_uav_rq7.php.
[2] https://www.bbc.com/news/business-45020853.

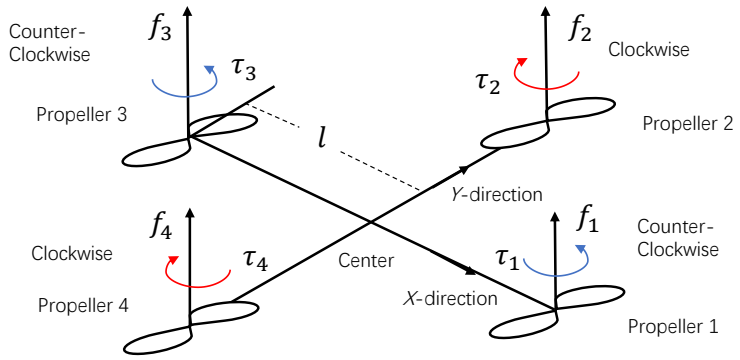

Figure 1.3: Quadrotor dynamics.

direction is achieved by increasing the rotational speed of propeller 4 and decreasing the speed of propeller 2. For the motion in Z-direction, the rotational speeds of all propellers increase or decrease equally, and then the total thrust moves the quadrotor upward or downward with balance. For the rotation around Z-direction with the hovering condition, one propeller pair increases the speed and another propeller pair decreases the speed, and then a torque around vertical direction is exerted. Therefore the quadrotor rotates around the vertical direction. In this case, all forces still remain balanced, so no altitude change occurs.

The quadrotor is a nonlinear system, and it is also an under-actuated system because the quadrotor has six degrees of freedom that are only actuated by four rotors. Due to its nonlinear dynamics and the under-actuated configuration, the controller design of the quadrotor is challenging. Therefore, it catches great attention in the field of control and robotics.

The quadrotor dynamics is concerned with how forces acting on the quadrotor influence its motion with respect to time. There are two general assumptions used for establishing the mathematical model of the quadrotor [12].

- The quadrotor is a rigid body.
- The center of the mass is located at the geometric center of the quadrotor.

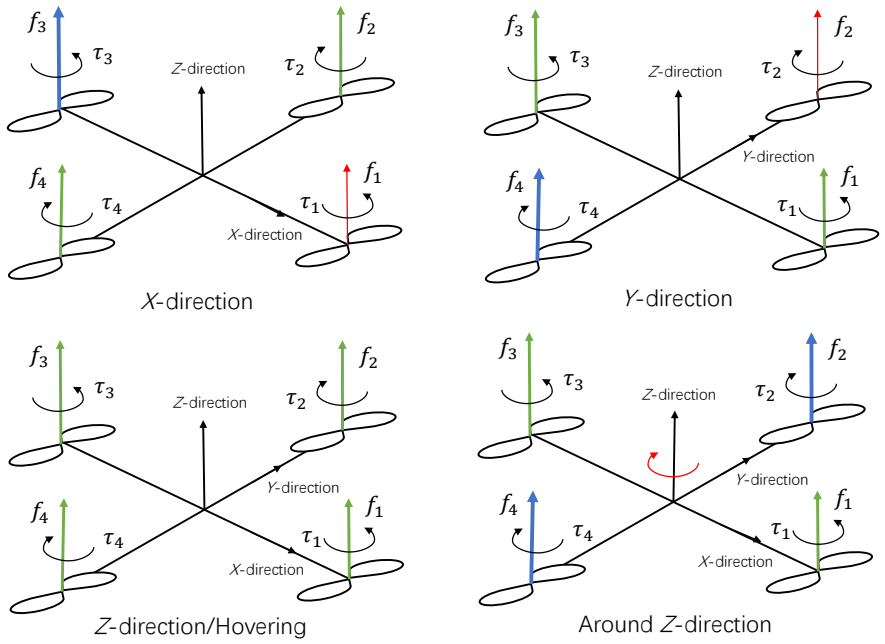

Figure 1.4: The relationship among forces, torques, and the movements.

There are a number of publications on modeling of quadrotor dynamics. Two methods commonly used for quadrotor modeling are Newton-Euler approach and Euler-Lagrange approach [13]. The former derives the model by using Newton's second law, while the latter derives the model upon conservation of energy.

The resulting models are typically nonlinear. However, when the quadrotor operates near the hover configuration, the nonlinear model can be approximated by a linearized one [14]. Since the linear model approximates the real system at the hover configuration, it may not provide a faithful description of the real system for a wide operating envelope. In contrast, the nonlinear model is accurate for a wide range of operation conditions, and yet it imposes complexity in the controller design [15].

1.3 Control of the Quadrotor

A variety of control methods have been proposed for the motion control of the quadrotor in the past decades. In this section, the recent works are reviewed.

1.3.1 Control Methods for the Nominal Quadrotor System

Early works consider the nominal model of the quadrotor, where the model is assumed to be an accurate representation of the quadrotor without any uncertainties. Selected linear and nonlinear methods, proportional-integral-derivative (PID) control, linear quadratic regulator control (LQR), sliding mode control, and backstepping control have been verified to be effective for motion control of the quadrotor.

PID control is widely used in the motion control of the quadrotor, which acts on applying a correction to the error value that is the difference between the desired state and the measured state. In [16], Salih *et al.* (2010) design PID controllers for two subsystems: a fully-actuated hover control subsystem and an under-actuated position control subsystem. The controllers are tuned by using the Zegler Nichols first method in this paper. The designed controllers stabilize the quadrotor and regulate it to a desired point. Although the structure of the PID controller is relatively simple, PID controller requires careful tuning of the controller parameters, which can be complex and time consuming [17]. LQR control, a well known modern optimal control method, gives a state feedback controller that provides good system performance. The controller is obtained by minimizing a quadratic cost function that is viewed as a linear combination of the weighted states and control inputs. The weighting matrices can be used as design parameters to penalize the state variables and the control signals [18]. In [19], Tosun *et al.* (2015) design classic LQR controllers for a quadrotor system that is divided into four subsystems: a height subsystem, a position subsystem, a pitch

and roll angle subsystem, and a yaw angle subsystem. The proposed controller is compared with PID controllers by the simulation results. Even though both methods steer the quadrotor to the desired position, the LQR controller has a lower control effort and a faster response.

On the other hand, a number of nonlinear control techniques have been successfully proposed according to the nonlinear quadrotor model. In [20], Xu *et al.* (2006) divide the whole quadrotor system into three subsystems: an under-actuated position subsystem, a fully-actuated altitude subsystem, and a fully-actuated yaw angle subsystem. The sliding mode controllers are developed for the yaw angle subsystem and position subsystem, while a rate bounded PID controller is designed for the altitude subsystem. The designed sliding mode controllers along with the PID controller are able to drive the quadrotor to the desired position with a desired yaw angle. In [21], a backstepping controller is developed by Madani *et al.* (2006) based on Lyapunov stability theory. The proposed controller can stabilize the quadrotor system and also control both the position on Z-axis and the yaw angle of the quadrotor.

1.3.2 Control Methods for the Quadrotor System with Uncertainties and Disturbances

When dealing with the nominal model, a number of controllers are employed to solve the problem and give satisfactory performances. However, the uncertainties are inevitable in many practical applications of the quadrotor. The model uncertainty is one type of uncertainties. The model uncertainty appears in the process of modeling, which is caused by the model mismatch between the ideal dynamics and real model and inaccurate system parameters. For example, the approximation of the nonlinear model causes the model uncertainty. The moment of inertia and the weight of quadrotor may change due to the variation in the payload [22], which also causes the model

uncertainty. Moreover, measurement noise is another type of uncertainty that should be considered in the controller design. The measurement noise typically results from deficiency of the sensors and its interference with other electrical instruments [23]. In such cases, designing a stabilizing controller becomes much more complicated. For example, a controller that is effective for the nominal system can not stabilize the system when the center of mass of quadrotor changes [24].

If the uncertainties are to be considered, more advanced control methods are needed. An LQR controller combined with Kalman filters is employed by Zhang *et al.* (2016) in [25]. A modified extended Kalman filter is added to the LQR controlled system to estimate the states where the measured values are affected by the uncertainties. It is verified that the proposed LQR controller rejects the state errors caused by the uncertainties. In [26], Astudillo *et al.* (2017) focus on the design of a combination of a linear quadratic Gaussian (LQG) controller and an H_∞ controller for the quadrotor position control. In LQG control, a state estimator estimates the states and rejects the model uncertainty, while a feedback gain enables the states to track the reference states. The H_∞ controller provides robustness against the external disturbances. The simulation results show that the proposed controllers can stabilize the quadrotor within a small region around the desired path. In [27], Kotaru *et al.* (2019) propose an L_1 adaptive controller on quadrotor attitude control in a nominal model. The L_1 controller includes a low-pass filter and a control law. The uncertainty caused by the difference between the real system and the nominal system is dealt with by the low-pass filter, while a desired system performance is achieved by the control law. The simulation results show a comparison between the performance of the L_1 controller and those under the nominal controller. It is verified that the L_1 controller can reject the uncertainties and maintain the performance.

The quadrotor is also extremely sensitive to external disturbances such as wind

disturbances when it autonomously flies under different flight conditions due to its lightweight [23]. Many control methods have been applied for the quadrotor exposed to external disturbances. In [28], Zhou *et al.* (2017) design a cascade PID controller for attitude control of the quadrotor. The controller consists of two parts: a PID controller for the stabilization of the quadrotor based on an inner-outer loop structure and a robust compensator for the external disturbance rejection. The experimental results show that the controlled quadrotor can track the attitude signals and reject the effect of wind disturbances. Labbadi *et al.* (2019) design a cascade of controllers for a quadrotor under the attendance of constant disturbances in [29]. The system has an inner-outer loop configuration. For the inner loop, a new robust sliding mode controller is developed to stabilize the attitude subsystem, and a backstepping controller is designed for the position subsystem. For the outer loop, an adaptive backstepping controller is developed for the altitude subsystem. It is verified that the proposed controllers can effectively hold the position of the quadrotor with the presence of external constant disturbances.

1.4 H_2-optimal Control Method

The H_2-optimal control problems is generally used for a linear, time invariant (LTI) system subject to bounded uncertainties and disturbances, and the H_2-optimal control method is used to design a controller to solve such problems. The following presents a brief review of the H_2-optimal control.

Consider a linear generalized control system as shown in Figure 1.5. Here $\boldsymbol{G}$ is the plant, $\boldsymbol{K}$ is the controller, $\boldsymbol{w} \in \mathbb{R}^h$ is a vector of all disturbance inputs, $\boldsymbol{u} \in \mathbb{R}^k$ is a vector of all control inputs, $\boldsymbol{y} \in \mathbb{R}^m$ is a vector consisting of measurement outputs, and $\boldsymbol{z} \in \mathbb{R}^r$ is a vector consisting of all required outputs [30]. The plant $\boldsymbol{G}$ is subjected

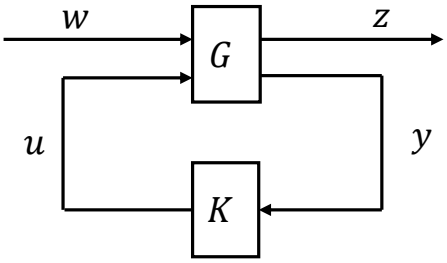

Figure 1.5: Generalized control system.

to uncertainties and disturbances, and $\boldsymbol{w}$ is assumed to be an appropriate signal set characterizing the uncertainties and disturbances.

Assume that the standard state-space representation of $\boldsymbol{G}$ is expressed as follows

$$\begin{aligned} \dot{\boldsymbol{x}} &= \boldsymbol{A}\boldsymbol{x} + \boldsymbol{B_1}\boldsymbol{w} + \boldsymbol{B_2}\boldsymbol{u}, \\ \boldsymbol{z} &= \boldsymbol{C_1}\boldsymbol{x} + \boldsymbol{D_{11}}\boldsymbol{w} + \boldsymbol{D_{12}}\boldsymbol{u}, \\ \boldsymbol{y} &= \boldsymbol{C_2}\boldsymbol{x} + \boldsymbol{D_{21}}\boldsymbol{w} + \boldsymbol{D_{22}}\boldsymbol{u}, \end{aligned} \tag{1.1}$$

where $\boldsymbol{A} \in \mathbb{R}^{n\times n}$, $\boldsymbol{B_1} \in \mathbb{R}^{n\times h}$, $\boldsymbol{B_2} \in \mathbb{R}^{n\times k}$, $\boldsymbol{C_1} \in \mathbb{R}^{r\times n}$, $\boldsymbol{C_2} \in \mathbb{R}^{m\times n}$, $\boldsymbol{D_{11}} \in \mathbb{R}^{r\times h}$, $\boldsymbol{D_{12}} \in \mathbb{R}^{r\times k}$, $\boldsymbol{D_{21}} \in \mathbb{R}^{m\times h}$, and $\boldsymbol{D_{22}} \in \mathbb{R}^{m\times k}$ are constant matrices, and $\boldsymbol{x} \in \mathbb{R}^n$ is the state variable [31].

A popular solution to this problem is the LQG control method. It is assumed that the disturbances and uncertainties are Gaussian in this method. An LQR control gain and a state estimator are designed separately. The estimator is used to estimate the states of the system from noisy measurements, while the LQR control gain is used to minimize the feedback error and confirm the performance. Lyapunov theory and Riccati equations lay the mathematical foundation for the LQG control method. The former, which is developed by A.M. Lyapunov (1892) [32], is studied for the stability of the dynamic systems [33], while the latter, which is first introduced by J.F. Riccati (1724) [34], is typically used in control area to find an optimal feedback

controller that minimizes the quadratic cost function [35]. The two-step scheme in LQG controller design is known as the separation principle. Since the estimator is designed relying on the open-loop estimation with respect to system uncertainties, the system stability cannot be guaranteed under various weighting parameter selection. The inappropriate weighting parameters may prevent the algorithm from finding a good solution to reduce the effects of the uncertainties, therefore destabilizing the system [36].

A significant change occurred in 1989, when Doyle *et al.* (1989) introduced the H_2-optimal control method [30]. The H_2-optimal control problem aims to find a feedback controller that stabilizes the system and minimizes the H_2 norm of the transfer function $\boldsymbol{T_{zw}}$. The solution is obtained by the state-space approach in the famous DGKF paper [30]. The H_2-optimal control method is an extension of the LQG control. For a system in a state-space form, under several assumptions on the controllability and observability of the system, an optimal controller is obtained by solving two algebraic Riccati equations like LQG control. Compared with LQG control, the H_2-optimal control is an interconnection of the estimator and the feedback controller. Furthermore, the weighting matrices of the estimator and the feedback controller are determined in the modeling process, instead of the controller design process [37]. In addition, the disturbances and uncertainties in the H_2-optimal problem can be colored noises [37].

In the following few years, varieties of approaches are proposed to solve the general H_2-optimal problem. In [38], Hunt *et al.* (1992) propose a polynomial equation approach that relies on the algebraic properties of polynomial matrices. The solution is derived based on the solvability of the polynomial matrix equations. In [39], Takaba *et al.* (1998) introduce a solution to the H_2-optimal problem for the system in a descriptor form. The solution is derived by using a standard model matching

technique. In recent years, the LMI approach appears to be the most popular method to deal with a flexible class of applications [40].

1.5 Contributions

In this thesis, a linearized quadrotor dynamic model of a specific quadrotor named QBall-X4 is employed. The aim is to design an control system using H_2-optimal control method for the motion control of the QBall-X4 quadrotor subject to disturbances and uncertainties. The contributions of this thesis are listed as follows.

- A linearized dynamic model of the quadrotor is derived.
- The LQR control method is introduced. For comparison purposes, a state feedback LQR controller is proposed for the nominal quadrotor model.
- The H_2-optimal control method is studied, and an H_2-optimal controller is developed for the quadrotor system under the uncertainty and disturbance.
- A comparison between the LQR controller and the H_2-optimal controller is evaluated by simulation results.

1.6 Organization of the Thesis

The remainder of the thesis is organized as follows.

- In Chapter 2, a detailed description of the experimental platform is given.
- In Chapter 3, the modeling of the quadrotor is presented, and a linearized model is obtained by using Euler-Lagrange approach.

- In Chapter 4, the implementation of LQR control on the X-position subsystem is investigated. A state feedback LQR controller is developed to operate the quadrotor from the original position to the desired position. The performance is illustrated by simulation results.

- In Chapter 5, the H_2-optimal control theory is studied. It begins with the derivation of the state-space approach to the H_2-optimal control problem. Furthermore, the LMI approach is provided. An H_2 state feedback controller is developed. The performance of the proposed H_2-optimal controller is evaluated by the simulation results and the experimental results.

- In Chapter 6, the conclusion remarks are provided, and some potential future works are recommended.

Chapter 2

Experimental Platform

2.1 Overview

The experimental platform employed in this thesis is Quanser Unmanned Vehicle System developed by Quanser [2]. The experimental platform is installed in the indoor environment. As shown in Figure 2.1, the experimental platform consists of three parts: a ground station, a QBall-X4 quadrotor and an OptiTrack motion capture system including multiple cameras manufactured by NaturalPoint Inc.

The remaining parts of this chapter are organized as follows. In Section 2.2, the software installed in the ground station is introduced. In Section 2.3, the structure of QBall-X4 quadrotor is provided. The indoor motion capture system, OptiTrack, is introduced in Section 2.4. Lastly, the conclusion of this chapter is drawn in Section 2.5.

2.2 Ground Station

The ground station is a host PC running Windows operating system. MATLAB Simulink, Quanser's QUARC real-time control software and Quanser's Motive soft-

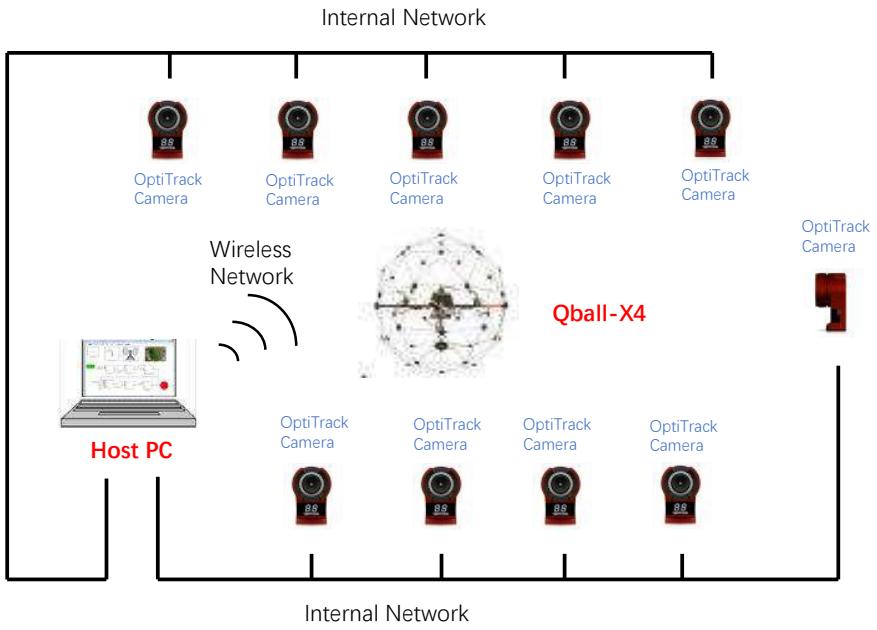

Figure 2.1: The layout of the experimental platform [1].

ware are installed in the host PC. QUARC serves as an interface between the Simulink and the QBall-X4 [2]. The controller is firstly created as a Simulink model, and then this Simulink model is compiled by QUARC to generate executable codes that can be directly implemented on the QBall-X4 quadrotor. Moreover, QUARC receives the sensor measurements from the quadrotor and sends them to Simulink. The Motive software processes the images captured by the multi-camera system, extracts the position information of the quadrotor, and sends it to Simulink. During the post-processing, Simulink receives all the state information from QUARC and the Motive software and stores the collected data.

The entire interconnection between the host PC and other elements is achieved by two types of networks. The OptiTrack cameras broadcast the images to Motive via an internal network. An ad-hoc peer-to-peer wireless TCP/IP connection is established between the host PC and the QBall-X4 via a wireless USB adapter [2]. An IP address of the QBall-X4 is provided by Quanser Inc, and the IP address of the host PC is set

within a valid range in order to connect to the local area network (LAN).

2.3 QBall-X4 Quadrotor

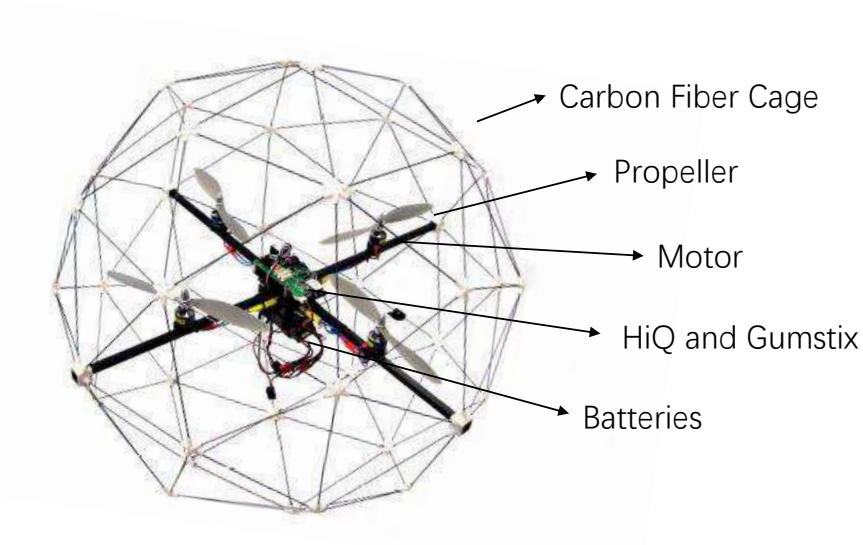

Figure 2.2: The configuration of the QBall-X4 [2].

Figure 2.2 shows the QBall-X4 quadrotor, which consists of four sets of motors and propellers, an embedded Gumstix computer, an HiQ data acquisition card, two batteries and a carbon fiber cage.

The propellers are actuated by the motors, while the motors are controlled by commands generated by the Gumstix computer. The Gumstix computer functions as an on-board controller, which executes the compiled executable codes to control the QBall-X4 quadrotor.

The HiQ DAQ card is the data acquisition board of the QBall-X4, which is mounted in the center of the QBall-X4 together with the embedded Gumstix computer. The HiQ card is equipped with several on-board sensors, such as gyroscope, accelerometer and magnetometer. The measurements from the gyroscope, accelerometer, and magnetometer are fused to provide the orientation information of the quadro-

tor. In addition, a sonar sensor mounted at the bottom of the QBall-X4 measures the altitude. The HiQ card collects the sensor measurements and sends them to the ground station via LAN.

The quadrotor is powered by two 3-cell 2500mAh LiPo batteries that are mounted under the HiQ card. The quadrotor is enclosed in a carbon fiber cage which protects the quadrotor form indoor laboratory hazards.

2.4 OptiTrack Motion Capture System

OptiTrack, a marker-based optical motion capture system developed by NaturalPoint, is employed to capture the motion of the QBall-X4. The system has three components: reflective markers, OptiTrack cameras, and the Motive software.

The reflective markers are attached to the carbon fiber cage of QBall-X4 in a geometrically asymmetrical manner shown in Figure 2.3. The QBall-X4 is considered as a rigid body, and the markers are clearly visible. The movement of QBall-X4 is tracked based on these reflected light detection by the cameras. A total of ten OptiTrack Flex 3 cameras are included in this system, which are mounted around the walls of the laboratory. All of the cameras are connected to Motive software by the internal network. The camera sensors collect the images of the reflective markers and send them to the Motive. Figure 2.4 shows the reflective markers captured by the cameras in Motive. The Motive receives the data from all of the cameras and provides the informations to users, such as the position and the orientation of the QBall-X4 [41]. The OptiTrack cameras need to be calibrated to block the undesired reflection spot. The coordinate system of the three dimensional space is also defined in the camera calibration procedure.

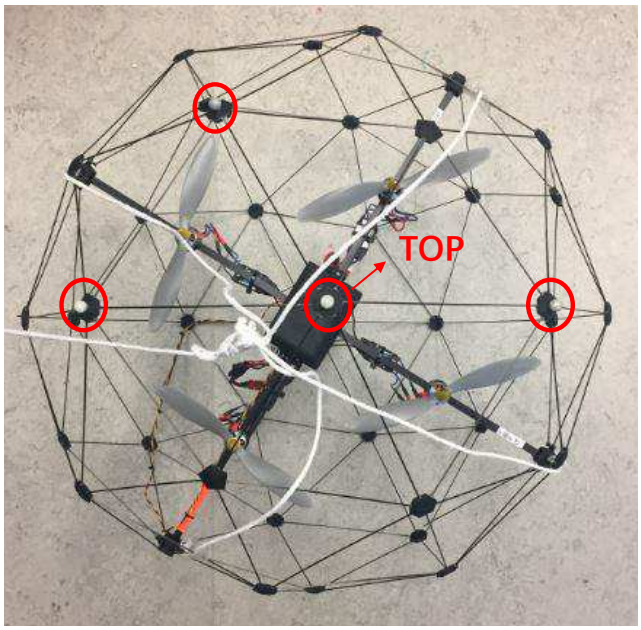

Figure 2.3: Placement of the reflection markers [2].

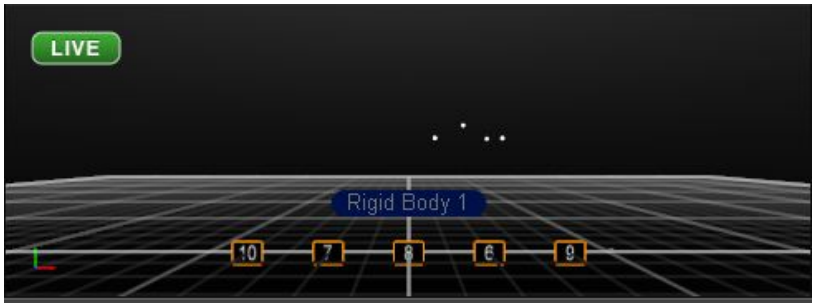

Figure 2.4: The reflective markers displayed in Motive [2].

2.5 Conclusion

This chapter introduces the overall experimental platform. The components of the experimental platform are presented in detail, including the ground station, the QBall-X4 quadrotor, and the OptiTrack motion caputure system. This platform provides a testing environment for the proposed controllers.

Chapter 3

Dynamic Model

3.1 Introduction

In this chapter, Euler-Lagrange approach is employed to derive the dynamic model of the quadrotor. The dynamic model is obtained under the assumptions that the quadrotor has a rigid symmetrical body, and the center of mass is located at the center of the quadrotor.

The rest of this chapter is organized as follows. Two reference coordinate frames and rotation matrices are introduced in Section 3.2. The Euler-Lagrange approach is derived in Section 3.3. In addition, the actuator dynamics that describes the forces resulting from the actuators is introduced in Section 3.4. Furthermore, the state-space dynamic model that involves quadrotor dynamics and actuator dynamics is developed in Section 3.5. In Section 3.6, the state-space dynamic model is decoupled into four subsystems known as the X-position subsystem, the Y-position subsystem, the altitude subsystem, and the yaw angle subsystem. The conclusion of this chapter is addressed in Section 3.7.

3.2 Reference Coordinate Frames and Rotation Matrices

Two coordinate frames are firstly defined prior to the derivation of dynamic model as shown in Figure 3.1. The first coordinate frame is the body attached frame, denoted by B frame. It is rigidly attached to the quadrotor, and its origin O_B is located at the center of gravity (COG) of the quadrotor. The X_B-axis and Y_B-axis are aligned with the arms of quadrotor, and the Z_B-axis is perpendicular to the X_BY_B plane and pointing upward. The second frame is the inertia frame, which is called the earth

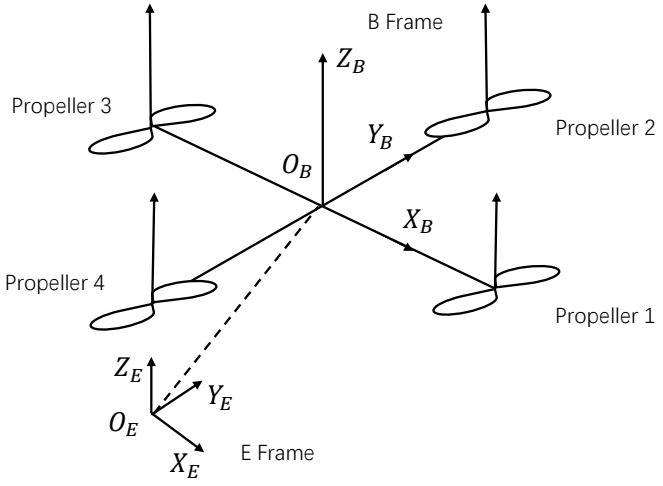

Figure 3.1: B frame and E frame.

fixed frame in this thesis, denoted by E frame. It is attached to the initial position of the quadrotor. The origin of E frame O_E is the origin of the body attached frame in the initial position, while the X_E-axis, Y_E-axis, and Z_E-axis are the initial positions of X_B-axis, Y_B-axis, and Z_B-axis, respectively.

The quadrotor has 6 degree of freedom (DOF). Define that the joint vector $\boldsymbol{q}$ is

composed of the position and the attitude as follows

$$\boldsymbol{q} = [X, Y, Z, \phi, \theta, \varphi]^\top , \tag{3.1}$$

where $[X, Y, Z]^\top$ is the position of the quadrotor with respect to the earth fixed frame, and $\boldsymbol{\eta} := [\phi, \theta, \varphi]^\top$ is the attitude of the quadrotor. ϕ, θ, ψ are referred to as roll, pitch, and yaw angles of the quadrotor, respectively.

The rotation matrix can be obtained by using the Euler angle convention [1], as the orientation of the body attached frame relative to the earth fixed frame can be specified by three Euler angles ϕ, θ, and ψ. Consider any rotation of the body attached frame with respect to the earth fixed frame as three successive rotations: Firstly, the quadrotor rotates around Z_B-axis by φ; then, the quadrotor rotates around Y_B-axis by θ; finally, the quadrotor rotates around X_B-axis by ϕ. Figure 3.2 shows the successive three rotations.

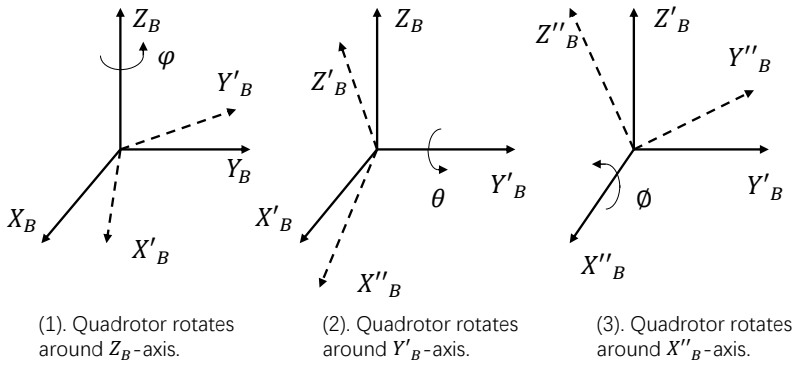

Figure 3.2: Three successive rotations.

It is observed that yaw angle φ, pitch angle θ, and roll angle ϕ are measured in the body attached frame. Therefore, the rotation matrix that denotes the orientation of

the body attached frame with respect to the earth fixed frame is obtained as follows

$$\begin{aligned}\boldsymbol{R} &= \boldsymbol{R_{Z,\varphi}}\boldsymbol{R_{Y,\theta}}\boldsymbol{R_{X,\phi}} \\ &= \begin{bmatrix} C_\varphi & -S_\varphi & 0 \\ S_\varphi & C_\varphi & 0 \\ 0 & 0 & 1 \end{bmatrix} \begin{bmatrix} C_\theta & 0 & S_\theta \\ 0 & 1 & 0 \\ -S_\theta & 0 & C_\theta \end{bmatrix} \begin{bmatrix} 1 & 0 & 0 \\ 0 & C_\phi & -S_\phi \\ 0 & S_\phi & C_\phi \end{bmatrix} \\ &= \begin{bmatrix} C_\varphi C_\theta & C_\varphi S_\theta S_\phi - S_\varphi C_\phi & C_\varphi S_\theta C_\phi + S_\varphi S_\phi \\ S_\varphi C_\theta & S_\varphi S_\theta S_\phi + C_\varphi C_\phi & S_\varphi S_\theta C_\phi - C_\varphi S_\phi \\ -S_\theta & C_\theta S_\phi & C_\theta C_\phi \end{bmatrix},\end{aligned} \tag{3.2}$$

where $\boldsymbol{R_{Z,\varphi}}$, $\boldsymbol{R_{Y,\theta}}$, and $\boldsymbol{R_{X,\phi}}$ are the rotation matrices describing the rotations through angle φ, θ, and ϕ around the Z_B-axis, Y_B-axis, and X_B-axis, respectively. S_ϕ, S_θ, S_φ, C_ϕ, C_θ, and C_φ are the space-saving trigonometric notation, which are exemplified by the expression $S_\phi = \sin\phi$ and $C_\phi = \cos\phi$.

Some variables such as the thrust forces, are measured with respect to B frame, while some variables such as the position of the quadrotor, are measured with respect to E frame. The rotation matrix $\boldsymbol{R}$ is used to transform the variables from B frame to E frame.

Define the angular velocity of the quadrotor expressed in B frame and the Euler angle rate $\dot{\boldsymbol{\eta}}$ as follows

$$\boldsymbol{\omega_B} := \begin{bmatrix} \omega_\phi \\ \omega_\theta \\ \omega_\varphi \end{bmatrix}, \dot{\boldsymbol{\eta}} = \begin{bmatrix} \dot{\phi} \\ \dot{\theta} \\ \dot{\varphi} \end{bmatrix}. \tag{3.3}$$

Since φ, θ, and ϕ are measured in the body attached frame, $\boldsymbol{\omega_B}$ can be described as

follows [42]

$$\boldsymbol{\omega_B} = \begin{bmatrix} \omega_\phi \\ \omega_\theta \\ \omega_\varphi \end{bmatrix} = \begin{bmatrix} \dot{\phi} \\ 0 \\ 0 \end{bmatrix} + \boldsymbol{R_{X,-\varphi}} \begin{bmatrix} 0 \\ \dot{\theta} \\ 0 \end{bmatrix} + \boldsymbol{R_{X,-\varphi} R_{Y,-\theta}} \begin{bmatrix} 0 \\ 0 \\ \dot{\varphi} \end{bmatrix} = \mathbf{W}_{\boldsymbol{\eta}} \dot{\boldsymbol{\eta}}, \tag{3.4}$$

where $\boldsymbol{R_{Z,-\varphi}}$, $\boldsymbol{R_{Y,-\theta}}$, and $\boldsymbol{R_{X,-\phi}}$ are the rotation matrices describing the rotations through angle $-\varphi$, $-\theta$, and $-\phi$ around the Z_B-axis, Y_B-axis, and X_B-axis, respectively, and

$$\mathbf{W}_{\boldsymbol{\eta}} = \begin{bmatrix} 1 & 0 & -S_\theta \\ 0 & C_\phi & S_\phi C_\theta \\ 0 & -S_\phi & C_\phi C_\theta \end{bmatrix}.$$

Assuming that pitch and roll angles are small enough, we have a simple approximation

$$\cos\theta = \cos\phi = 1,\ \sin\theta = \sin\phi = 0, \tag{3.5}$$

so $\mathbf{W}_{\boldsymbol{\eta}}$ can be simplified as an identity matrix.

3.3 Euler-Lagrange Approach

The kinetic energy KE of the quadrotor is the summation of the translational kinetic energy and rotational kinetic energy as follows [43]

$$KE = \frac{1}{2} m \boldsymbol{v_E}^\top \boldsymbol{v_E} + \frac{1}{2} \boldsymbol{\omega_E}^\top \boldsymbol{\mathcal{I}} \boldsymbol{\omega_E}, \tag{3.6}$$

where m is the mass of the quadrotor, $\boldsymbol{\mathcal{I}}$ is the inertia tensor, and $\boldsymbol{v_E}$ and $\boldsymbol{\omega_E}$ are the velocity and the angular velocity of the quadrotor expressed in E frame, respectively. The inertia tensor $\boldsymbol{\mathcal{I}}$ is also expressed in the earth fixed frame.

The inertia tensor is difficult to be computed in the earth fixed frame, however, the inertia matrix expressed in the body attached frame is a constant matrix. The inertia matrix $\boldsymbol{\mathcal{I}}$ is related to its counterpart in B frame $\boldsymbol{I_B}$ by [43]:

$$\boldsymbol{\mathcal{I}} = \boldsymbol{R}\boldsymbol{I_B}\boldsymbol{R}^\top. \tag{3.7}$$

Then, the kinetic energy KE is derived as follows

$$\begin{aligned} KE &= \frac{1}{2}m\boldsymbol{v_E}^\top\boldsymbol{v_E} + \frac{1}{2}\boldsymbol{\omega_E}^\top\boldsymbol{R}\boldsymbol{I_B}\boldsymbol{R}^\top\boldsymbol{\omega_E} \\ &= \frac{1}{2}m\boldsymbol{v_E}^\top\boldsymbol{v_E} + \frac{1}{2}(\boldsymbol{R}^\top\boldsymbol{\omega_E})^\top\boldsymbol{I_B}(\boldsymbol{R}^\top\boldsymbol{\omega_E}) \\ &= \frac{1}{2}m\boldsymbol{v_E}^\top\boldsymbol{v_E} + \frac{1}{2}\boldsymbol{\omega_B}^\top\boldsymbol{I_B}\boldsymbol{\omega_B}, \end{aligned} \tag{3.8}$$

where $\boldsymbol{\omega_B}$ is the angular velocity expressed in the body attached frame. Substituting (3.4) into (3.8), we have

$$KE = \frac{1}{2}m\boldsymbol{v_E}^\top\boldsymbol{v_E} + \frac{1}{2}(\mathbf{W}_{\boldsymbol{\eta}}\dot{\boldsymbol{\eta}})^\top\boldsymbol{I_B}(\mathbf{W}_{\boldsymbol{\eta}}\dot{\boldsymbol{\eta}}) = \frac{1}{2}m\boldsymbol{v_E}^\top\boldsymbol{v_E} + \frac{1}{2}\dot{\boldsymbol{\eta}}^\top\boldsymbol{I_B}\dot{\boldsymbol{\eta}}. \tag{3.9}$$

The potential energy PE is calculated as follows

$$PE = mgZ, \tag{3.10}$$

where g denotes gravitational constant.

Since the structure of the quadrotor is symmetrical, the inertial matrix $\boldsymbol{I_B}$ can be described as a diagonal matrix as follows

$$\boldsymbol{I_B} = \begin{bmatrix} I_{xx} & 0 & 0 \\ 0 & I_{yy} & 0 \\ 0 & 0 & I_{zz} \end{bmatrix}, \tag{3.11}$$

where I_{xx}, I_{yy}, and I_{zz} are the moment of inertia of the quadrotor in X_B-axis, Y_B-axis, and Z_B-axis, respectively.

Therefore, using the equations of the kinetic energy KE and the potential energy PE, (i.e., (3.9)-(3.10)), the Lagrangian L_{EL} can be obtained as follows

$$\begin{aligned} L_{EL} =& KE - PE \\ =& \frac{1}{2}m\dot{X}^2 + \frac{1}{2}m\dot{Y}^2 + \frac{1}{2}m\dot{Z}^2 + \frac{1}{2}I_{xx}\dot{\phi}^2 + \frac{1}{2}I_{yy}\dot{\theta}^2 + \frac{1}{2}I_{zz}\dot{\varphi}^2 - mgZ. \end{aligned} \tag{3.12}$$

Let $\boldsymbol{F_E}$ be the generalized force in the earth fixed frame associated with the thrust, and let $\boldsymbol{F_B}$ be the force in the body attached frame generated by the rotors. The thrusts which are generated by the propellers are denoted by f_1, f_2, f_3, f_4, as shown in Figure 1.3. The other forces, such as centrifugal force, centripetal force, and drag force, and so on, are neglected. According to the Euler angle convention and the rotation matrix $\boldsymbol{R}$, it yields

$$\boldsymbol{F_E} = \boldsymbol{R}\boldsymbol{F_B} = \boldsymbol{R}\begin{bmatrix} 0 \\ 0 \\ F_z \end{bmatrix} = \begin{bmatrix} (C_\varphi S_\theta C_\phi + S_\varphi S_\phi)F_z \\ (S_\varphi S_\theta C_\phi - C_\varphi S_\phi)F_z \\ C_\theta C_\phi F_z \end{bmatrix}, \tag{3.13}$$

where $F_z = f_1 + f_2 + f_3 + f_4$ is the total thrust.

Define $\boldsymbol{\tau_\eta}$ as the torque

$$\boldsymbol{\tau_\eta} := [\tau_\phi \ \tau_\theta \ \tau_\varphi]^\top. \tag{3.14}$$

By substituting (3.2), (3.12)-(3.14) into the Euler-Lagrange equation

$$\frac{d}{dt}\left(\frac{\partial L_{EL}}{\partial \dot{q}}\right) - \frac{\partial L_{EL}}{\partial q} = \begin{bmatrix} \boldsymbol{F_E} \\ \boldsymbol{\tau_\eta} \end{bmatrix}, \tag{3.15}$$

the dynamic model of the quadrotor is derived as follows

$$\begin{cases} \ddot{X} = \dfrac{1}{m}(C_\varphi S_\theta C_\phi + S_\varphi S_\phi)F_z \\ \ddot{Y} = \dfrac{1}{m}(S_\varphi S_\theta C_\phi - C_\varphi S_\phi)F_z \\ \ddot{Z} = -g + \dfrac{1}{m}C_\theta C_\phi F_z \\ \ddot{\phi} = \dfrac{\tau_\phi}{I_{xx}} \\ \ddot{\theta} = \dfrac{\tau_\theta}{I_{yy}} \\ \ddot{\varphi} = \dfrac{\tau_\varphi}{I_{zz}} \end{cases} . \tag{3.16}$$

The dynamic model (3.16) is a nonlinear model. In order to perform the linearization, we assume that:

- The quadrotor operates near the hover position, which means that $\mathbf{W}_{\boldsymbol{\eta}}$ is approximately an identity matrix as discussed before.
- The quadrotor hovers in the air, which means that F_z=mg.
- Pitch, roll, and yaw angles are small. The small angle approximation is applied, which means that $\sin\phi \approx \phi$, $\sin\theta \approx \theta$, $\sin\varphi \approx \varphi$, $\cos\phi \approx 1$, $\cos\theta \approx 1$, and $\cos\varphi \approx 1$.

Therefore, the linearized model is obtained as:

$$\begin{cases} \ddot{X} = g\theta \\ \ddot{Y} = -g\phi \\ \ddot{Z} = -g + \dfrac{F_z}{m} \\ \ddot{\phi} = \dfrac{\tau_\phi}{I_{xx}} \\ \ddot{\theta} = \dfrac{\tau_\theta}{I_{yy}} \\ \ddot{\varphi} = \dfrac{\tau_\varphi}{I_{zz}} \end{cases}. \tag{3.17}$$

3.4 Actuator Dynamics

As mentioned before, the thrusts and torques are related to the rotational speed of propellers. Each propeller is controlled by an independent pulse width modulation (PWM) signal. In this section, the relation between PWM signals and the thrusts and torques are presented.

The thrust generated by each propeller is modeled by the following frequency domain equation

$$f_i(s) = K_f \frac{\delta}{s+\delta} u_i, \tag{3.18}$$

where u_i represents the PWM input to the rotors, f_i is the thrust, $i = 1, 2, 3, 4$, δ denotes the motor bandwidth, and K_f is a positive gain [2]. Defining $\triangle f_i$ be the change of the thrust f_i, and define $\triangle u_i$ be the PWM signal that causes $\triangle f_i$, then

$$\triangle f_i(s) = K_f \frac{\delta}{s+\delta} \triangle u_i. \tag{3.19}$$

The rotation around the Z_B-axis is generated by the reaction torques. The rotation around Y_B-axis is generated by the pair thrusts (f_1, f_3), and the rotation around X_B-

axis is generated by (f_2, f_4). Figure 3.3 shows a model of the motion in Y_B-axis as an example.

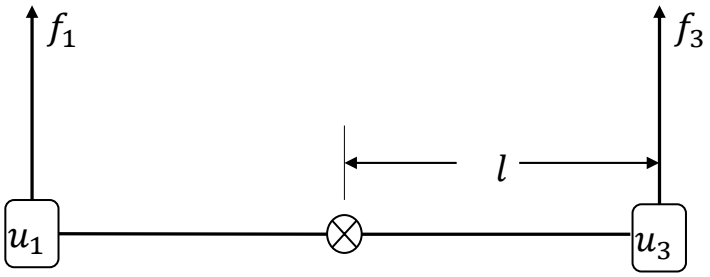

Figure 3.3: A model in Y_B-axis.

Therefore, the torque is given by

$$\boldsymbol{\tau_\eta} = \begin{bmatrix} \tau_\phi \\ \tau_\theta \\ \tau_\varphi \end{bmatrix} = \begin{bmatrix} (f_2 - f_4)l \\ (f_1 - f_3)l \\ \tau_1 + \tau_3 - \tau_2 - \tau_4 \end{bmatrix}, \tag{3.20}$$

where τ_1, τ_2, τ_3, τ_4 denote the reaction torques as shown in Figure 1.3.

Suppose that the pitch angle is caused by the $\triangle f_1$ and $\triangle f_3$ pair with an equal value. Define u_θ as a PWM control input that causes $\triangle f_1$. The pitch torque τ_θ is given by

$$\tau_\theta = (f_1 - f_3)l = 2 \triangle f_1 l = 2K_f l \frac{\delta}{s+\delta} u_\theta. \tag{3.21}$$

Similarly, about the X_B-axis, the roll torque τ_ϕ is given by

$$\tau_\phi = 2K_f l \frac{\delta}{s+\delta} u_\phi, \tag{3.22}$$

where u_ϕ denotes a PWM control input related to the change of roll angel ϕ.

The total thrust is generated by four rotors. Suppose the changes in all PWM

inputs are equal, then the total trust is given by

$$F_z = \sum_{i=1}^{4} \triangle f_i = 4K_f \frac{\delta}{s+\delta} u_z, \tag{3.23}$$

where u_z is the control input which is the change in the PWM input to one rotor.

Suppose the changes in all reaction torque are equal, which are described by the first-order function

$$\triangle \tau_i = K_y u_\varphi, \tag{3.24}$$

where u_φ is the change in the PWM input that causes the change of the reaction torque, $i = 1, 2, 3, 4$, and K_y is a positive gain for the reaction torque. Then, the yaw torque τ_φ is described by following equation

$$\tau_\varphi = \tau_1 + \tau_3 - \tau_2 - \tau_4 = 4K_y u_\varphi. \tag{3.25}$$

Defining $[v_\phi,\ v_\theta,\ v_\varphi,\ v_z]^\top$ as a state variable representing the actuator dynamics, the linear dynamic model for the actuator in state-space form is written as follows

$$\begin{aligned}
\begin{bmatrix} \dot{v}_\phi \\ \dot{v}_\theta \\ \dot{v}_\varphi \\ \dot{v}_z \end{bmatrix} &= \begin{bmatrix} -\delta & 0 & 0 & 0 \\ 0 & -\delta & 0 & 0 \\ 0 & 0 & 0 & 0 \\ 0 & 0 & 0 & -\delta \end{bmatrix} \begin{bmatrix} v_\phi \\ v_\theta \\ v_\varphi \\ v_z \end{bmatrix} + \begin{bmatrix} \delta & 0 & 0 & 0 \\ 0 & \delta & 0 & 0 \\ 0 & 0 & 0 & 0 \\ 0 & 0 & 0 & \delta \end{bmatrix} \begin{bmatrix} u_\phi \\ u_\theta \\ u_\varphi \\ u_z \end{bmatrix}, \\
\begin{bmatrix} \tau_\phi \\ \tau_\theta \\ \tau_\varphi \\ F_z \end{bmatrix} &= \begin{bmatrix} 2K_f l & 0 & 0 & 0 \\ 0 & 2K_f l & 0 & 0 \\ 0 & 0 & 0 & 0 \\ 0 & 0 & 0 & 4K_f \end{bmatrix} \begin{bmatrix} v_\phi \\ v_\theta \\ v_\varphi \\ v_z \end{bmatrix} + \begin{bmatrix} 0 & 0 & 0 & 0 \\ 0 & 0 & 0 & 0 \\ 0 & 0 & \delta & 0 \\ 0 & 0 & 0 & 0 \end{bmatrix} \begin{bmatrix} u_\phi \\ u_\theta \\ u_\varphi \\ u_z \end{bmatrix}.
\end{aligned} \tag{3.26}$$

The values of the system parameters are given in Table 3.1 [2].

Parameter	Value	Description
K_f	120 N	Positive gain for the thrust model
K_y	4 N·m	Positive gain for the reaction torque model
δ	15 rad/s	Motor bandwidth
m	1.4 kg	Mass of the quadrotor
l	0.2 m	Length of the arm
I_{xx}	0.03 kg· m^2	Moment of inertia of the quadrotor about X_B-axis
I_{yy}	0.03 kg· m^2	Moment of inertia of the quadrotor about Y_B-axis
I_{zz}	0.04 kg· m^2	Moment of inertia of the quadrotor about Z_B-axis

Table 3.1: System parameters.

3.5 State-space Model Involving Quadrotor Dynamics and Actuator Dynamics

Substitute (3.26) to (3.17). The state-space model involving quadrotor dynamics and actuator dynamics is derived as follows

$$\begin{aligned}
\dot{\boldsymbol{X}}_{\boldsymbol{x}} &= \boldsymbol{A}_{\boldsymbol{x}}\boldsymbol{X}_{\boldsymbol{x}} + \boldsymbol{B}_{\boldsymbol{x}}\theta, \\
\dot{\boldsymbol{X}}_{\boldsymbol{\theta}} &= \boldsymbol{A}_{\boldsymbol{\theta}}\boldsymbol{X}_{\boldsymbol{\theta}} + \boldsymbol{B}_{\boldsymbol{\theta}}u_\theta, \\
\dot{\boldsymbol{X}}_{\boldsymbol{y}} &= \boldsymbol{A}_{\boldsymbol{y}}\boldsymbol{X}_{\boldsymbol{y}} + \boldsymbol{B}_{\boldsymbol{x}}\phi, \\
\dot{\boldsymbol{X}}_{\boldsymbol{\phi}} &= \boldsymbol{A}_{\boldsymbol{\phi}}\boldsymbol{X}_{\boldsymbol{\phi}} + \boldsymbol{B}_{\boldsymbol{\phi}}u_\phi, \\
\dot{\boldsymbol{X}}_{\boldsymbol{z}} &= \boldsymbol{A}_{\boldsymbol{z}}\boldsymbol{X}_{\boldsymbol{z}} + \boldsymbol{B}_{\boldsymbol{x}}u_z + \boldsymbol{\Omega}, \\
\dot{\boldsymbol{X}}_{\boldsymbol{\varphi}} &= \boldsymbol{A}_{\boldsymbol{\varphi}}\boldsymbol{X}_{\boldsymbol{\varphi}} + \boldsymbol{B}_{\boldsymbol{\varphi}}u_\varphi,
\end{aligned} \tag{3.27}$$

where

$$\boldsymbol{X_x} = \begin{bmatrix} X \\ \dot{X} \end{bmatrix}, \boldsymbol{A_x} = \begin{bmatrix} 0 & 1 \\ 0 & 0 \end{bmatrix}, \boldsymbol{B_x} = \begin{bmatrix} 0 \\ g \end{bmatrix},$$

$$\boldsymbol{X_\theta} = \begin{bmatrix} \theta \\ \dot{\theta} \\ v_\theta \end{bmatrix}, \boldsymbol{A_\theta} = \begin{bmatrix} 0 & 1 & 0 \\ 0 & 0 & \frac{2K_f l}{I_{yy}} \\ 0 & 0 & -\delta \end{bmatrix}, \boldsymbol{B_\theta} = \begin{bmatrix} 0 \\ 0 \\ \delta \end{bmatrix},$$

$$\boldsymbol{X_y} = \begin{bmatrix} Y \\ \dot{Y} \end{bmatrix}, \boldsymbol{A_y} = \begin{bmatrix} 0 & 1 \\ 0 & 0 \end{bmatrix}, \boldsymbol{B_y} = \begin{bmatrix} 0 \\ -g \end{bmatrix},$$

$$\boldsymbol{X_\phi} = \begin{bmatrix} \phi \\ \dot{\phi} \\ v_\phi \end{bmatrix}, \boldsymbol{A_\phi} = \begin{bmatrix} 0 & 1 & 0 \\ 0 & 0 & \frac{2K_f l}{I_{xx}} \\ 0 & 0 & -\delta \end{bmatrix}, \boldsymbol{B_\phi} = \begin{bmatrix} 0 \\ 0 \\ \delta \end{bmatrix},$$

$$\boldsymbol{X_z} = \begin{bmatrix} Z \\ \dot{Z} \\ v_z \end{bmatrix}, \boldsymbol{A_z} = \begin{bmatrix} 0 & 1 & 0 \\ 0 & 0 & \frac{4K_f}{m} \\ 0 & 0 & -\delta \end{bmatrix}, \boldsymbol{B_z} = \begin{bmatrix} 0 \\ 0 \\ \delta \end{bmatrix}, \boldsymbol{\Omega} = \begin{bmatrix} 0 \\ -g \\ 0 \end{bmatrix},$$

$$\boldsymbol{X_\varphi} = \begin{bmatrix} \varphi \\ \dot{\varphi} \end{bmatrix}, \boldsymbol{A_\varphi} = \begin{bmatrix} 0 & 1 \\ 0 & 0 \end{bmatrix}, \boldsymbol{B_\varphi} = \begin{bmatrix} 0 \\ \frac{4K_y}{I_{zz}} \end{bmatrix}.$$

3.6 Decoupled System

Obviously the yaw motion of the quadrotor is realized by the signal u_φ, and the motions along X-axis, Y-axis, and Z-axis are realized by the control signals u_θ, u_ϕ, and u_z, respectively. Suppose that the cross-coupling is removed by neglecting all the gyroscopic effects. The system model is split into four subsystems as follows.

X-position subsystem

$$\begin{aligned} \dot{\boldsymbol{X}}_{\boldsymbol{x}} &= \boldsymbol{A}_{\boldsymbol{x}}\boldsymbol{X}_{\boldsymbol{x}} + \boldsymbol{B}_{\boldsymbol{x}}\theta, \\ \dot{\boldsymbol{X}}_{\boldsymbol{\theta}} &= \boldsymbol{A}_{\boldsymbol{\theta}}\boldsymbol{X}_{\boldsymbol{\theta}} + \boldsymbol{B}_{\boldsymbol{\theta}}u_{\theta}, \end{aligned} \tag{3.28}$$

Y-position subsystem

$$\begin{aligned} \dot{\boldsymbol{X}}_{\boldsymbol{y}} &= \boldsymbol{A}_{\boldsymbol{y}}\boldsymbol{X}_{\boldsymbol{y}} + \boldsymbol{B}_{\boldsymbol{x}}\phi, \\ \dot{\boldsymbol{X}}_{\boldsymbol{\phi}} &= \boldsymbol{A}_{\boldsymbol{\phi}}\boldsymbol{X}_{\boldsymbol{\phi}} + \boldsymbol{B}_{\boldsymbol{\phi}}u_{\phi}, \end{aligned} \tag{3.29}$$

yaw angle subsystem

$$\dot{\boldsymbol{X}}_{\boldsymbol{\varphi}} = \boldsymbol{A}_{\boldsymbol{\varphi}}\boldsymbol{X}_{\boldsymbol{\varphi}} + \boldsymbol{B}_{\boldsymbol{\varphi}}u_{\varphi}, \tag{3.30}$$

and altitude subsystem

$$\dot{\boldsymbol{X}}_{\boldsymbol{z}} = \boldsymbol{A}_{\boldsymbol{z}}\boldsymbol{X}_{\boldsymbol{z}} + \boldsymbol{B}_{\boldsymbol{x}}u_{z} + \boldsymbol{\Omega}. \tag{3.31}$$

Due to the symmetrical geometry of the quadrotor, the Y-position subsystem is similar to the X-position subsystem. In this thesis, the controllers are developed for the X-position subsystem; similar methods can also be used for the Y-position subsystem.

Rewrite (3.28) in a state-space form

$$\begin{aligned} \dot{\boldsymbol{X}}_{\boldsymbol{X}} &= \boldsymbol{A}_{\boldsymbol{X}}\boldsymbol{X}_{\boldsymbol{X}} + \boldsymbol{B}_{\boldsymbol{X}}u_{\theta}, \\ \boldsymbol{Y}_{\boldsymbol{X}} &= \boldsymbol{C}_{\boldsymbol{X}}\boldsymbol{X}_{\boldsymbol{X}}, \end{aligned} \tag{3.32}$$

where

$$\boldsymbol{X_X} = \begin{bmatrix} X \\ \dot{X} \\ \theta \\ \dot{\theta} \\ v_\theta \end{bmatrix}, \ \boldsymbol{A_X} = \begin{bmatrix} 0 & 1 & 0 & 0 & 0 \\ 0 & 0 & g & 0 & 0 \\ 0 & 0 & 0 & 1 & 0 \\ 0 & 0 & 0 & 0 & \frac{2K_f l}{I_{yy}} \\ 0 & 0 & 0 & 0 & -\delta \end{bmatrix}, \ \boldsymbol{B_X} = \begin{bmatrix} 0 \\ 0 \\ 0 \\ 0 \\ \delta \end{bmatrix},$$

and $\boldsymbol{C_X}$ is an identity matrix $\boldsymbol{I_5}$.

3.7 Conclusion

This chapter introduces the dynamic model used in the motion control of the quadrotor. Firstly, some prerequisite concepts are introduced, including reference coordinate frames, Euler angles, and rotation matrices. Then, the dynamic model of the quadrotor is derived by using Euler-Lagrange approach. Next, the actuator dynamics is also introduced. After that, the state-space model of the quadrotor is presented by combining the quadrotor dynamics and actuator dynamics. Finally, the decoupled dynamics is introduced.

Chapter 4

LQR Controller Design for the Quadrotor

4.1 Introduction

In this chapter, the LQR control method for the continuous-time system is firstly introduced. The LQR control, as a typical optimal method, aims at finding a feedback controller to minimize the quadratic cost which is related to the weighted state variables and weighted control inputs. Then, an LQR controller is employed to regulate the quadrotor from the initial position to the desired position. Finally, the simulation results verify the effectiveness of the proposed controller.

The rest of this chapter is organized as follows. The LQR control method is introduced in Section 4.2. The application of state feedback LQR control method to the position subsystem of the quadrotor is discussed in Section 4.3.

4.2 LQR Controller Design

Assume that there is no uncertainty and disturbance, and the plant is a nominal plant as follows [42]

$$\begin{aligned} \dot{\boldsymbol{x}} &= \boldsymbol{A}\boldsymbol{x} + \boldsymbol{B}\boldsymbol{u}, \\ \boldsymbol{z} &= \boldsymbol{C}\boldsymbol{x}, \end{aligned} \tag{4.1}$$

where $\boldsymbol{x} \in \mathbb{R}^n$ is the state, $\boldsymbol{u} \in \mathbb{R}^k$ is the input, $\boldsymbol{z} \in \mathbb{R}^n$ is the output, $\boldsymbol{A} \in \mathbb{R}^{n\times n}$, $\boldsymbol{B} \in \mathbb{R}^{n\times k}$, $\boldsymbol{C} \in \mathbb{R}^{n\times n}$ are constant matrices, and $\boldsymbol{C}$ is identity matrix $\boldsymbol{I_n}$.

The quadratic cost function of this system is given by

$$J_{lqr} = \int_0^\infty (\boldsymbol{x}^\top \boldsymbol{Q_{lqr}} \boldsymbol{x} + \boldsymbol{u}^\top \boldsymbol{R_{lqr}} \boldsymbol{u}) dt, \tag{4.2}$$

where $\boldsymbol{Q_{lqr}} \in \mathbb{R}^{n\times n}$ and $\boldsymbol{R_{lqr}} \in \mathbb{R}^{k\times k}$ are symmetric, positive definite matrices. $\boldsymbol{x}^\top \boldsymbol{Q_{lqr}} \boldsymbol{x}$ is related to the energy of the controlled output, while $\boldsymbol{u}^\top \boldsymbol{R_{lqr}} \boldsymbol{u}$ denotes the weighted energy of the control signal.

Define the Hamiltonian function as follows

$$H_{lqr} = \frac{1}{2}(\boldsymbol{x}^\top \boldsymbol{Q_{lqr}} \boldsymbol{x} + \boldsymbol{u}^\top \boldsymbol{R_{lqr}} \boldsymbol{u}) + \boldsymbol{\lambda}^\top (\boldsymbol{A}\boldsymbol{x} + \boldsymbol{B}\boldsymbol{u}), \tag{4.3}$$

where $\boldsymbol{\lambda} \in \mathbb{R}^n$ is the Lagrange multiplier.

Following Pontryagin's maximum principle [44, 45], we have

$$\begin{aligned} &\frac{dH_{lqr}}{d\boldsymbol{u}} = \frac{1}{2}\boldsymbol{u}^\top \boldsymbol{R_{lqr}} + \frac{1}{2}\boldsymbol{u}^\top \boldsymbol{R_{lqr}^\top} + \boldsymbol{\lambda}^\top \boldsymbol{B} = \boldsymbol{0} \Rightarrow \quad \boldsymbol{u} = -\boldsymbol{R_{lqr}^{-1}} \boldsymbol{B}^\top \boldsymbol{\lambda}, \\ &(\frac{dH_{lqr}}{d\boldsymbol{x}})^\top = (\frac{1}{2}\boldsymbol{x}^\top \boldsymbol{Q_{lqr}} + \frac{1}{2}\boldsymbol{x}^\top \boldsymbol{Q_{lqr}^\top} + \boldsymbol{\lambda}^\top \boldsymbol{A})^\top = \boldsymbol{Q_{lqr}}\boldsymbol{x} + \boldsymbol{A}^\top \boldsymbol{\lambda} = -\dot{\boldsymbol{\lambda}}. \end{aligned} \tag{4.4}$$

Define

$$\boldsymbol{\lambda} = \boldsymbol{P_{lqr}} \boldsymbol{x}. \tag{4.5}$$

Taking the derivative of (4.5), we have

$$\begin{aligned} \dot{\boldsymbol{\lambda}} &= \dot{\boldsymbol{P}}_{\boldsymbol{lqr}}\boldsymbol{x} + \boldsymbol{P}_{\boldsymbol{lqr}}\dot{\boldsymbol{x}} = \dot{\boldsymbol{P}}_{\boldsymbol{lqr}}\boldsymbol{x} + \boldsymbol{P}_{\boldsymbol{lqr}}\boldsymbol{A}\boldsymbol{x} - \boldsymbol{P}_{\boldsymbol{lqr}}\boldsymbol{B}\boldsymbol{R}_{\boldsymbol{lqr}}^{-1}\boldsymbol{B}^{\top}\boldsymbol{\lambda} \\ \Rightarrow \quad -\dot{\boldsymbol{P}}_{\boldsymbol{lqr}} &= \boldsymbol{P}_{\boldsymbol{lqr}}\boldsymbol{A} + \boldsymbol{A}^{\top}\boldsymbol{P}_{\boldsymbol{lqr}} - \boldsymbol{P}_{\boldsymbol{lqr}}\boldsymbol{B}\boldsymbol{R}_{\boldsymbol{lqr}}^{-1}\boldsymbol{B}^{\top}\boldsymbol{P}_{\boldsymbol{lqr}} + \boldsymbol{Q}_{\boldsymbol{lqr}}. \end{aligned} \tag{4.6}$$

Assuming that the control law takes the form

$$\boldsymbol{u} = -\boldsymbol{K}_{\boldsymbol{lqr}}\boldsymbol{x}, \tag{4.7}$$

the control gain $\boldsymbol{K}_{\boldsymbol{lqr}}$ is given by

$$\boldsymbol{K}_{\boldsymbol{lqr}} = \boldsymbol{R}_{\boldsymbol{lqr}}^{-1}\boldsymbol{B}^{\top}\boldsymbol{P}_{\boldsymbol{lqr}}, \tag{4.8}$$

where $\boldsymbol{P}_{\boldsymbol{lqr}}$ is the unique solution of the algebraic Riccati equation [45]

$$\boldsymbol{A}^{\top}\boldsymbol{P}_{\boldsymbol{lqr}} + \boldsymbol{P}_{\boldsymbol{lqr}}\boldsymbol{A} - \boldsymbol{P}_{\boldsymbol{lqr}}\boldsymbol{B}\boldsymbol{R}_{\boldsymbol{lqr}}^{-1}\boldsymbol{B}^{\top}\boldsymbol{P}_{\boldsymbol{lqr}} + \boldsymbol{Q}_{\boldsymbol{lqr}} = \boldsymbol{0}. \tag{4.9}$$

To verify the stability, the closed-loop system is derived as follows

$$\dot{\boldsymbol{x}} = \boldsymbol{A}\boldsymbol{x} + \boldsymbol{B}(-\boldsymbol{K}_{\boldsymbol{lqr}}\boldsymbol{x}) = (\boldsymbol{A} - \boldsymbol{B}\boldsymbol{K}_{\boldsymbol{lqr}})\boldsymbol{x}. \tag{4.10}$$

Define a candidate Lyapunov function of the closed-loop system as

$$V_{lqr}(\boldsymbol{x}) = \boldsymbol{x}^{\top}\boldsymbol{P}_{\boldsymbol{lqr}}\boldsymbol{x}. \tag{4.11}$$

Taking the derivative of (4.11), it yields

$$\begin{aligned}\dot{V}_{lqr} &= \dot{\boldsymbol{x}}^\top \boldsymbol{P_{lqr}} \boldsymbol{x} + \boldsymbol{x}^\top \boldsymbol{P_{lqr}} \dot{\boldsymbol{x}} \\ &= (\boldsymbol{A} - \boldsymbol{B}\boldsymbol{K_{lqr}})^\top \boldsymbol{P_{lqr}} \boldsymbol{x} + \boldsymbol{x}^\top \boldsymbol{P_{lqr}} (\boldsymbol{A} - \boldsymbol{B}\boldsymbol{K_{lqr}}) \\ &= \boldsymbol{x}^\top (-\boldsymbol{Q_{lqr}} - \boldsymbol{P_{lqr}} \boldsymbol{B} \boldsymbol{R_{lqr}^{-1}} \boldsymbol{B}^\top \boldsymbol{P_{lqr}}) \boldsymbol{x}.\end{aligned} \tag{4.12}$$

Since $\boldsymbol{R_{lqr}}$ and $\boldsymbol{Q_{lqr}}$ are positive definite, $\boldsymbol{Q_{lqr}} + \boldsymbol{P_{lqr}} \boldsymbol{B} \boldsymbol{R_{lqr}^{-1}} \boldsymbol{B}^\top \boldsymbol{P_{lqr}}$ is positive definite. It means that $\dot{V}_{lqr}$ is positive. Therefore, the closed-loop system is asymptotically stable [46].

The weighting matrix selection reflects the optimal performance of the LQR controller. Basically, the larger value of $\boldsymbol{Q_{lqr}}$ means that the system is stabilized with smaller changes in the states. Similarly, choosing a large value for $\boldsymbol{R_{lqr}}$ means that the system is stabilized with a small control signal. The Bryson's rule is a popular method to determine the weighting matrices [47]. According to this rule, the weighting matrices are chosen to be diagonal matrices. The diagonal elements of the weighting matrices $\boldsymbol{Q_{lqr}}$ and $\boldsymbol{R_{lqr}}$ are the reciprocals of the squares of the maximum acceptable values of the states and the input control signals, respectively. Another popular method is to minimize the quadratic cost function with output weight [48]. Based on this method, the weighting matrix $\boldsymbol{Q_{lqr}}$ is selected as $\boldsymbol{C}^\top \boldsymbol{C}$, and the weighting matrix $\boldsymbol{R_{lqr}}$ is selected as $\rho \boldsymbol{I_k}$, where the scalar $\rho > 0$.

4.3 LQR Controller Design for the Position Subsystem of the Quadrotor

4.3.1 Simulation Setup

To design the LQR controller, the plant should be a nominal dynamic model. The position subsystem of the quadrotor (3.31) previously discussed is a nominal model as follows

$$\dot{\boldsymbol{x}} = \boldsymbol{A}\boldsymbol{x} + \boldsymbol{B}\boldsymbol{u}_{\boldsymbol{\theta}},$$
$$\boldsymbol{z} = \boldsymbol{C}\boldsymbol{x},$$

where

$$\boldsymbol{A} = \boldsymbol{A}_{\boldsymbol{X}},\ \boldsymbol{B} = \boldsymbol{B}_{\boldsymbol{X}},\ \boldsymbol{C} = \boldsymbol{C}_{\boldsymbol{X}}. \tag{4.13}$$

Define that $\boldsymbol{x_d} = [x_r, 0, 0, 0, 0]^\top$ is the desired state, where x_r is the desired position along the X_E-axis.

The purpose of the controller is to regulate the quadrotor from the initial state to the desired state by minimizing the cost. Let the state error be $\boldsymbol{e_d} = \boldsymbol{x} - \boldsymbol{x_d}$ and the system output be $\boldsymbol{z_d}$. Then, the error dynamics can be derived as

$$\begin{aligned} \dot{\boldsymbol{e}}_{\boldsymbol{d}} &= \dot{\boldsymbol{x}} - \dot{\boldsymbol{x}}_{\boldsymbol{d}} = \boldsymbol{A}\boldsymbol{x} + \boldsymbol{B}\boldsymbol{u}_{\boldsymbol{\theta}} - \boldsymbol{A}\boldsymbol{x}_{\boldsymbol{d}} = \boldsymbol{A}\boldsymbol{e}_{\boldsymbol{d}} + \boldsymbol{B}\boldsymbol{u}_{\boldsymbol{\theta}}, \\ \boldsymbol{z}_{\boldsymbol{d}} &= \boldsymbol{z} - \boldsymbol{C}\boldsymbol{e}_{\boldsymbol{d}} = \boldsymbol{C}\boldsymbol{e}_{\boldsymbol{d}}. \end{aligned} \tag{4.14}$$

Considering the error dynamic system in (4.14), the LQR controller can be designed as

$$\boldsymbol{u}_{\boldsymbol{\theta}} = -\boldsymbol{K}_{\boldsymbol{lqr}}\boldsymbol{e}_{\boldsymbol{d}} = -\boldsymbol{K}_{\boldsymbol{lqr}}(\boldsymbol{x} - \boldsymbol{x}_{\boldsymbol{d}}), \tag{4.15}$$

where $\boldsymbol{K}_{\boldsymbol{lqr}}$ is the LQR control gain that can be calculated by (4.8).

The closed-loop system is derived as follows

$$\begin{aligned}\dot{\boldsymbol{x}} &= \boldsymbol{A}\boldsymbol{x} + \boldsymbol{B}(-\boldsymbol{K}_{\boldsymbol{lqr}}(\boldsymbol{x} - \boldsymbol{x}_{\boldsymbol{d}})) \\ &= \boldsymbol{A}\boldsymbol{x} - \boldsymbol{B}\boldsymbol{K}_{\boldsymbol{lqr}}\boldsymbol{x} + \boldsymbol{B}\boldsymbol{K}_{\boldsymbol{lqr}}\boldsymbol{x}_{\boldsymbol{d}} \\ &= (\boldsymbol{A} - \boldsymbol{B}\boldsymbol{K}_{\boldsymbol{lqr}})\boldsymbol{x} + \boldsymbol{B}\boldsymbol{K}_{\boldsymbol{lqr}}\boldsymbol{x}_{\boldsymbol{d}}.\end{aligned} \tag{4.16}$$

4.3.2 Simulation Results

Suppose that the initial state of the quadrotor $\boldsymbol{x_0}$ is $[0.5, 0, 0, 0, 0]^\top$, and the desired state is $[0, 0, 0, 0, 0]^\top$. The weighting matrix $\boldsymbol{Q_{lqr}}$ and $\boldsymbol{R_{lqr}}$ are selected as $\boldsymbol{C}^\top\boldsymbol{C}$ and $\rho\boldsymbol{I_1}$, respectively. Taking different values of ρ, we compare the simulation results.

Figure 4.1 shows the trajectories of the position and the pitch angle of the quadrotor. While $\boldsymbol{Q_{lqr}}$ is held as a constant matrix, the convergence speed of state is affected by the scalar ρ in the weighting matrix $\boldsymbol{R_{lqr}}$. The larger the value of ρ is, the slower the state response is.

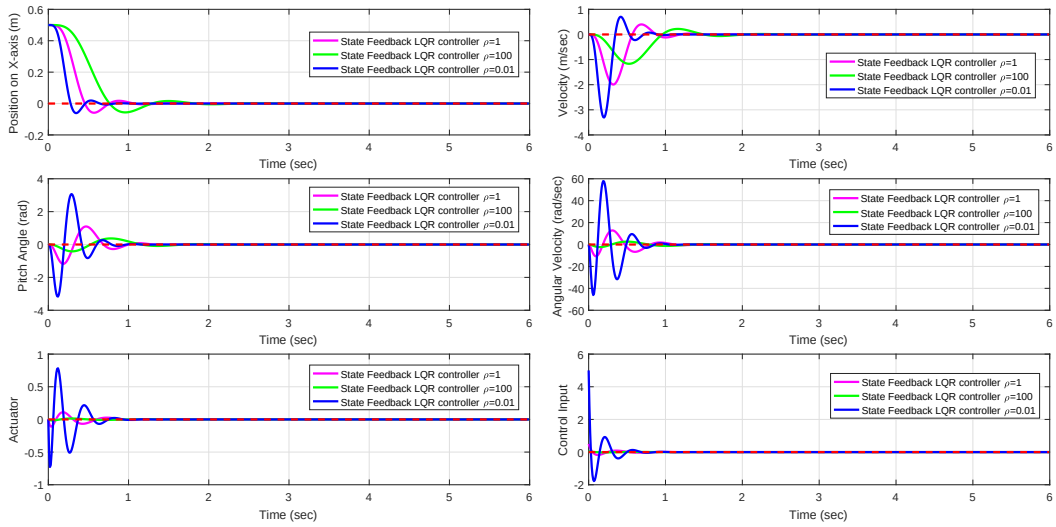

Figure 4.1: Simulation results of the state feedback LQR controller.

4.4 Conclusion

This chapter introduces the LQR problem and presents a derivation of general LQR controller. A state feedback LQR controller is then designed for the position regulation of the quadrotor. Simulation results are provided to verify the effectiveness of the proposed controller.

Chapter 5

H_2-optimal Controller Design for the Quadrotor

5.1 Introduction

Consider a finite dimensional LTI system with the state-space form

$$\begin{aligned} \dot{\boldsymbol{x}}_{\boldsymbol{o}} &= \boldsymbol{A}_{\boldsymbol{o}}\boldsymbol{x}_{\boldsymbol{o}} + \boldsymbol{B}_{\boldsymbol{o}}\boldsymbol{u}_{\boldsymbol{o}}, \\ \boldsymbol{z}_{\boldsymbol{o}} &= \boldsymbol{C}_{\boldsymbol{o}}\boldsymbol{x}_{\boldsymbol{o}}. \end{aligned} \tag{5.1}$$

where $\boldsymbol{x}_{\boldsymbol{o}} \in \mathbb{R}^n$ is the state, $\boldsymbol{u}_{\boldsymbol{o}} \in \mathbb{R}^k$ is the input, $\boldsymbol{z}_{\boldsymbol{o}} \in \mathbb{R}^n$ is the output, $\boldsymbol{A}_{\boldsymbol{o}} \in \mathbb{R}^{n\times n}$, $\boldsymbol{B}_{\boldsymbol{o}} \in \mathbb{R}^{n\times k}$, $\boldsymbol{C}_{\boldsymbol{o}} \in \mathbb{R}^{r\times n}$ are constant matrices.

Define $\boldsymbol{P}_{\boldsymbol{c}}$ and $\boldsymbol{P}_{\boldsymbol{o}}$ as follows

$$\begin{aligned} \boldsymbol{P}_{\boldsymbol{c}} &= \int_0^\infty e^{\boldsymbol{A}_{\boldsymbol{o}}t}\boldsymbol{B}_{\boldsymbol{o}}\boldsymbol{B}_{\boldsymbol{o}}^\top e^{\boldsymbol{A}_{\boldsymbol{o}}^\top t}dt, \\ \boldsymbol{P}_{\boldsymbol{o}} &= \int_0^\infty e^{\boldsymbol{A}_{\boldsymbol{o}}^\top t}\boldsymbol{C}_{\boldsymbol{o}}^\top\boldsymbol{C}_{\boldsymbol{o}}e^{\boldsymbol{A}_{\boldsymbol{o}}t}dt. \end{aligned} \tag{5.2}$$

The H_2-norm of transfer function $\boldsymbol{T_o}$ of (5.1) is calculated as follows

$$\begin{aligned} ||\boldsymbol{T_o}||_2^2 &= \frac{1}{2\pi}\int_{-\infty}^{\infty} \text{Trace}\left[\boldsymbol{T_o}(j\omega)^\top \boldsymbol{T_o}(j\omega)\right] d\omega \\ &= \int_0^{\infty} \text{Trace}\left[\left[\boldsymbol{C_o}e^{\boldsymbol{A_o}t}\boldsymbol{B_o}\right]^\top \left[\boldsymbol{C_o}e^{\boldsymbol{A_o}t}\boldsymbol{B_o}\right]\right] dt \\ &= \text{Trace}\left[\boldsymbol{B_o}^\top \int_0^{\infty} e^{\boldsymbol{A_o}^\top t}\boldsymbol{C_o}^\top \boldsymbol{C_o}e^{\boldsymbol{A_o}t}dt\boldsymbol{B_o}\right] \\ &= \text{Trace}\left[\boldsymbol{B_o}^\top \boldsymbol{P_o}\boldsymbol{B_o}\right] \end{aligned} \tag{5.3}$$

or

$$\begin{aligned} ||\boldsymbol{T_o}||_2^2 &= \frac{1}{2\pi}\int_{-\infty}^{\infty} \text{Trace}\left[\boldsymbol{T_o}(j\omega)\boldsymbol{T_o}(j\omega)^\top\right] d\omega \\ &= \int_0^{\infty} \text{Trace}\left[\left[\boldsymbol{C_o}e^{\boldsymbol{A_o}t}\boldsymbol{B_o}\right] \left[\boldsymbol{C_o}e^{\boldsymbol{A_o}t}\boldsymbol{B_o}\right]^\top\right] dt \\ &= \text{Trace}\left[\boldsymbol{C_o} \int_0^{\infty} e^{\boldsymbol{A_o}t}\boldsymbol{B_o}\boldsymbol{B_o}^\top e^{\boldsymbol{A_o}^\top t}dt\boldsymbol{C_o}^\top\right] \\ &= \text{Trace}\left[\boldsymbol{C_o}\boldsymbol{P_c}\boldsymbol{C_o}^\top\right]. \end{aligned} \tag{5.4}$$

$\boldsymbol{P_o}$ is the observability Gramian, satisfying the filter-type Lyapunov equation

$$\boldsymbol{A_o}^\top \boldsymbol{P_o} + \boldsymbol{P_o}\boldsymbol{A_o} + \boldsymbol{C_o}^\top \boldsymbol{C_o} = \boldsymbol{0}. \tag{5.5}$$

Similarly, $\boldsymbol{P_c}$ is the reachability Gramian, satisfying the control-type Lyapunov equation [33, 49]

$$\boldsymbol{A_o}\boldsymbol{P_c} + \boldsymbol{P_c}\boldsymbol{A_o}^\top + \boldsymbol{B_o}\boldsymbol{B_o}^\top = \boldsymbol{0}. \tag{5.6}$$

As we discussed before, the block diagram in Figure 1.5 shows the generalized

control system with disturbances. The plant P is described by the state-space form

$$\begin{aligned} \dot{\boldsymbol{x}} &= \boldsymbol{A}\boldsymbol{x} + \boldsymbol{B_1}\boldsymbol{w} + \boldsymbol{B_2}\boldsymbol{u}, \\ \boldsymbol{z} &= \boldsymbol{C_1}\boldsymbol{x} + \boldsymbol{D_{11}}\boldsymbol{w} + \boldsymbol{D_{12}}\boldsymbol{u}, \\ \boldsymbol{y} &= \boldsymbol{C_2}\boldsymbol{x} + \boldsymbol{D_{21}}\boldsymbol{w} + \boldsymbol{D_{22}}\boldsymbol{u}, \end{aligned} \tag{5.7}$$

where $\boldsymbol{A} \in \mathbb{R}^{n\times n}$, $\boldsymbol{B_1} \in \mathbb{R}^{n\times h}$, $\boldsymbol{B_2} \in \mathbb{R}^{n\times k}$, $\boldsymbol{C_1} \in \mathbb{R}^{r\times n}$, $\boldsymbol{C_2} \in \mathbb{R}^{m\times n}$, $\boldsymbol{D_{11}} \in \mathbb{R}^{r\times h}$, $\boldsymbol{D_{12}} \in \mathbb{R}^{r\times k}$, $\boldsymbol{D_{21}} \in \mathbb{R}^{m\times h}$, $\boldsymbol{D_{22}} \in \mathbb{R}^{m\times k}$, $\boldsymbol{x} \in \mathbb{R}^n$ is the state variable, $\boldsymbol{w} \in \mathbb{R}^h$ is the disturbance input, $\boldsymbol{u} \in \mathbb{R}^k$ is the control input, $\boldsymbol{y} \in \mathbb{R}^m$ is the measurement output, and $\boldsymbol{z} \in \mathbb{R}^r$ is the required output [31].

Suppose that the controller $\boldsymbol{K}$ has a state-space form as follows

$$\begin{aligned} \dot{\boldsymbol{x}}_{\boldsymbol{k}} &= \boldsymbol{A_k}\boldsymbol{x_k} + \boldsymbol{B_k}\boldsymbol{y}, \\ \boldsymbol{u} &= \boldsymbol{C_k}\boldsymbol{x_k} + \boldsymbol{D_k}\boldsymbol{y}, \end{aligned} \tag{5.8}$$

and has the control law

$$\boldsymbol{u} = \boldsymbol{K}\boldsymbol{y}. \tag{5.9}$$

Assuming that $\boldsymbol{D_{22}} = \boldsymbol{0}$, the transfer function $\boldsymbol{T_{zw}}$ from $\boldsymbol{w}$ to $\boldsymbol{z}$ therefore has a state-space form as

$$\boldsymbol{T_{zw}} = \left[\begin{array}{c|c} \boldsymbol{A_c} & \boldsymbol{B_c} \\ \hline \boldsymbol{C_c} & \boldsymbol{D_c} \end{array}\right] \tag{5.10}$$

or

$$\begin{aligned} \dot{\boldsymbol{x}}_{\boldsymbol{c}} &= \boldsymbol{A_c}\boldsymbol{x_c} + \boldsymbol{B_c}\boldsymbol{w}, \\ \boldsymbol{z} &= \boldsymbol{C_c}\boldsymbol{x_c} + \boldsymbol{D_c}\boldsymbol{w}, \end{aligned} \tag{5.11}$$

where

$$
\begin{aligned}
\boldsymbol{x_c} &= \begin{bmatrix} \boldsymbol{x} \\ \boldsymbol{x_k} \end{bmatrix}, \\
\boldsymbol{A_c} &= \begin{bmatrix} \boldsymbol{A} + \boldsymbol{B_2 D_k C_2} & \boldsymbol{B_2 C_k} \\ \boldsymbol{B_k C_2} & \boldsymbol{A_k} \end{bmatrix}, \\
\boldsymbol{B_c} &= \begin{bmatrix} \boldsymbol{B_1} + \boldsymbol{B_2 D_k D_{21}} \\ \boldsymbol{B_k D_{21}} \end{bmatrix}, \\
\boldsymbol{C_c} &= \begin{bmatrix} \boldsymbol{C_1} + \boldsymbol{D_{12} D_k C_2} & \boldsymbol{D_{12} C_k} \end{bmatrix}, \\
\boldsymbol{D_c} &= \boldsymbol{D_{11}} + \boldsymbol{D_{12} D_k D_{21}}.
\end{aligned}
\tag{5.12}
$$

The H_2-optimal problem is defined as finding a controller $\boldsymbol{K}$ to stabilize the system and minimize the H_2-norm of the transfer function from $\boldsymbol{w}$ to $\boldsymbol{z}$ when $\boldsymbol{D_c} = \boldsymbol{0}$ [50].

$$
\text{minimize} \quad ||\boldsymbol{T_{zw}}||_2^2. \tag{5.13}
$$

Equation (5.11) has the same form as (5.1) when $\boldsymbol{D_c} = \boldsymbol{0}$. Therefore, the objective of an H_2-optimal problem for (5.7) is to find an appropriate $\boldsymbol{P_o}$ or $\boldsymbol{P_c}$ for the transfer function $\boldsymbol{T_{zw}}$.

The rest of this chapter is organized as follows. The existence of H_2-optimal controller is discussed in Section 5.2. The state-space approach and LMI approach for solving the H_2-optimal problem are provided in Section 5.3 and Section 5.4, respectively. The H_2-optimal methods are applied to the X-position subsystem of the quadrotor in Section 5.5. The experimental results are provided in Section 5.6.

5.2 Assumptions Related to the H_2-optimal Control Problem

The following assumptions must be satisfied to guarantee the existence of an H_2-optimal controller K:

1) $\boldsymbol{D_{11}} = \mathbf{0}$. This is assumed that the direct feedforward matrix from $\boldsymbol{w}$ to $\boldsymbol{z}$ is equal to zero, which means that we can obtain an H_2 norm of the closed-loop transfer function from $\boldsymbol{w}$ to $\boldsymbol{z}$ [49]. If this matrix is not equal to zero, a transformation can be used to transfer the problem with $\boldsymbol{D_{11}} \neq \mathbf{0}$ to an equivalent problem with a new $\boldsymbol{D_{11}} = \mathbf{0}$ [51].

2) $\boldsymbol{D_{22}} = \mathbf{0}$. We also assume that the direct feedforward matrix from $\boldsymbol{u}$ to $\boldsymbol{y}$ is equal to zero. It means that the closed-loop system always has a zero gain at infinite frequency, or there exits the closed-loop transfer matrix [31].

3) $(\boldsymbol{A}, \boldsymbol{B_2})$ is stabilizable, and $(\boldsymbol{C_2}, \boldsymbol{A})$ is detectable. There exists a matrix $\boldsymbol{F}$ such that all eigenvalues of $\boldsymbol{A} + \boldsymbol{B_2F}$ have negative real part, or $\boldsymbol{A} + \boldsymbol{B_2F}$ is a Hurwitz matrix. There also exists a matrix $\boldsymbol{L}$ such that $\boldsymbol{A} + \boldsymbol{LC_2}$ is a Hurwitz matrix. If $\boldsymbol{A} + \boldsymbol{B_2F}$ and $\boldsymbol{A} + \boldsymbol{LC_2}$ are Hurwitz matrices, the system is stable. This assumption guarantees that two algebraic Riccati equations, which will be discussed fully later in this chapter, have unique solutions when we derive the results via state-space approaches [52].

4) $\boldsymbol{D_{12}}$ has full column rank, while $\boldsymbol{D_{21}}$ has full row rank. This condition guarantees that the controller is proper [53].

5) The matrix

$$\begin{bmatrix} \boldsymbol{A} - j\omega & \boldsymbol{B_2} \\ \boldsymbol{C_1} & \boldsymbol{D_{12}} \end{bmatrix} \quad \text{and} \quad \begin{bmatrix} \boldsymbol{A} - j\omega & \boldsymbol{B_1} \\ \boldsymbol{C_2} & \boldsymbol{D_{21}} \end{bmatrix}$$

have the full column rank and the full row rank at every frequency, respectively. This means that the disturbance input $\boldsymbol{w}$ affects the measured output $\boldsymbol{y}$ dependently for all ω, and the control input $\boldsymbol{u}$ should affect the performance output $\boldsymbol{z}$ for all ω. This condition guarantees that there are no control singularity and sensor singularity at all frequencies [54].

6) $\boldsymbol{D_{12}^\top C_1} = \mathbf{0}$ and $\boldsymbol{C_1^\top D_{12}} = \mathbf{0}$. This assumption is used to simplify the solution, which can be relaxed in other approaches, e.g., LMI methods, to solve the H_2-optimal problem [49].

5.3 State-space Solution to the H_2-optimal Control Problem

The H_2-optimal problem can be reduced to an LQG problem, where the colored noise can be considered as a white noise with a shaping filter [55]. The design of the H_2-optimal controller includes the design of an LQR controller for a nominal model which is not affected by the uncertainties and the design of a linear quadratic estimator (LQE) which estimates the states under the uncertainties and disturbances. The solution follows the separation principle, which means that the optimal LQR controller and the optimal LQE can be designed independently.

5.3.1 LQR Controller Design for the Full Information Subproblem

Assuming that all real states of the system are known, the general system is described as a full information system

$$\begin{aligned} \dot{\boldsymbol{x}} &= \boldsymbol{A}\boldsymbol{x} + \boldsymbol{B_1}\boldsymbol{w} + \boldsymbol{B_2}\boldsymbol{u}, \\ \boldsymbol{z} &= \boldsymbol{C_1}\boldsymbol{x} + \boldsymbol{D_{12}}\boldsymbol{u}, \end{aligned} \tag{5.14}$$

where a control feedback gain $\boldsymbol{F}$ can minimize the cost of the transfer function from $\boldsymbol{w}$ to $\boldsymbol{z}$ and stabilize the system. As the measured states are exactly equal to the real states in the full information problem, we have $\boldsymbol{y} = \boldsymbol{x}$ and $\boldsymbol{u} = \boldsymbol{F}\boldsymbol{y} = \boldsymbol{F}\boldsymbol{x}$.

The full information system (5.14) therefore can be described as

$$\begin{aligned} \dot{\boldsymbol{x}} &= \boldsymbol{A}\boldsymbol{x} + \boldsymbol{B_1}\boldsymbol{w} + \boldsymbol{B_2}\boldsymbol{u}, \\ \boldsymbol{z} &= \boldsymbol{C_1}\boldsymbol{x} + \boldsymbol{D_{12}}\boldsymbol{u}, \\ \boldsymbol{y} &= \boldsymbol{I}\boldsymbol{x}, \end{aligned} \tag{5.15}$$

where $\boldsymbol{I}$ is the identity matrix.

The closed-loop system is given by

$$\begin{aligned} \dot{\boldsymbol{x}} &= (\boldsymbol{A} + \boldsymbol{B_2}\boldsymbol{F})\boldsymbol{x} + \boldsymbol{B_1}\boldsymbol{w}, \\ \boldsymbol{z} &= (\boldsymbol{C_1} + \boldsymbol{D_{12}}\boldsymbol{F})\boldsymbol{x}, \end{aligned} \tag{5.16}$$

which can be described in a compact form

$$\boldsymbol{G_c} = \left[\begin{array}{c|c} \boldsymbol{A} + \boldsymbol{B_2}\boldsymbol{F} & \boldsymbol{B_1} \\ \hline \boldsymbol{C_1} + \boldsymbol{D_{12}}\boldsymbol{F} & \boldsymbol{0} \end{array}\right]. \tag{5.17}$$

Based on (5.3) and (5.5), the optimal objective of the full information problem is to minimize the H_2-norm of the transfer function of $\boldsymbol{G_c}$

$$||\boldsymbol{G_c}||_2^2 = \text{Trace}(\boldsymbol{B_1^\top P_o B_1}), \tag{5.18}$$

where $\boldsymbol{P_o}$ satisfies the following Lyapunov equation

$$(\boldsymbol{A} + \boldsymbol{B_2 F})^\top \boldsymbol{P_o} + \boldsymbol{P_o}(\boldsymbol{A} + \boldsymbol{B_2 F}) + (\boldsymbol{C_1} + \boldsymbol{D_{12} F})^\top (\boldsymbol{C_1} + \boldsymbol{D_{12} F}) = \boldsymbol{0}. \tag{5.19}$$

Define $\boldsymbol{Q_o} = \boldsymbol{C_1^\top C_1}$ and $\boldsymbol{R_o} = \boldsymbol{D_{12}^\top D_{12}}$. The cost function of (5.16) can be described as

$$\int_0^\infty (\boldsymbol{z}^\top \boldsymbol{z}) dt = \int_0^\infty ((\boldsymbol{C_1 x} + \boldsymbol{D_{12} F x})^\top (\boldsymbol{C_1 x} + \boldsymbol{D_{12} F x})) dt. \tag{5.20}$$

Define a substitute system

$$\begin{aligned} \dot{\boldsymbol{x}} &= \boldsymbol{A x} + \boldsymbol{B_2 u}, \\ \boldsymbol{z} &= \boldsymbol{C_1 x} \end{aligned} \tag{5.21}$$

with the same cost as (5.20). Via the LQR method, the cost function can be minimized, and the control gain $\boldsymbol{F}$ can be obtained by

$$\boldsymbol{F} = -\boldsymbol{R_o^{-1} B_2^\top X_o} = -(\boldsymbol{D_{12}^\top D_{12}})^{-1} \boldsymbol{B_2^\top X_o}, \tag{5.22}$$

where $\boldsymbol{X_o}$ is the unique solution of the algebraic Riccati equation

$$\boldsymbol{A^\top X_o} + \boldsymbol{X_o A} - \boldsymbol{X_o B_2 R_o^{-1} B_2^\top X_o} + \boldsymbol{Q_o} = \boldsymbol{0}. \tag{5.23}$$

Rewrite (5.22) as

$$-\boldsymbol{R_o F} = \boldsymbol{B_2^\top X_o^\top} = (\boldsymbol{X_o B_2})^\top. \tag{5.24}$$

Substituting (5.24) to (5.23), we can obtain that

$$\begin{aligned}
& \boldsymbol{A^\top X_o + X_o A - X_o B_2 R_o^{-1} B_2^\top X_o + Q_o = 0}. \\
\Rightarrow \quad & \boldsymbol{A^\top X_o + X_o A + Q_o + F^\top R_o F - F^\top R_o F - F^\top R_o^\top F = 0} \\
\Rightarrow \quad & \boldsymbol{A^\top X_o + X_o A + C_1^\top C_1 + F^\top D_{12}^\top D_{12} F + F^\top B_2^\top X_o + X_o B_2 F = 0} \\
\Rightarrow \quad & \boldsymbol{(A + B_2 F)^\top X_o + X_o (A + B_2 F) + (C_1 + D_{12} F)^\top (C_1 + D_{12} F) = 0}.
\end{aligned} \tag{5.25}$$

Therefore, the cost of (5.15) is minimized by the controller

$$\boldsymbol{F} = -(\boldsymbol{D_{12}^\top D_{12}})^{-1} \boldsymbol{B_2^\top X_o}, \tag{5.26}$$

and the optimal value is obtained by minimizing

$$||\boldsymbol{G_c}||_2^2 = \text{Trace}(\boldsymbol{B_1^\top X_o B_1}), \tag{5.27}$$

where $\boldsymbol{X_o}$ is the unique symmetric positive solution to the algebraic Riccati equation

$$\boldsymbol{A^\top X_o + X_o A - X_o B_2 (D_{12}^\top D_{12})^{-1} B_2^\top X_o + C_1^\top C_1 = 0}. \tag{5.28}$$

5.3.2 LQE Design for the Output Estimation Subproblem

Assuming that we now only have the measured output $\boldsymbol{y}$ of the system, the states of the system can be estimated based on the measured output. The general system can

be adjusted to the output estimation problem

$$\begin{aligned} \dot{\boldsymbol{x}} &= \boldsymbol{A}\boldsymbol{x} + \boldsymbol{B_1}\boldsymbol{w} + \boldsymbol{B_2}\boldsymbol{u}, \\ \hat{\boldsymbol{y}} &= \boldsymbol{C_1}\hat{\boldsymbol{x}} + \boldsymbol{D_{12}}\boldsymbol{u}, \\ \boldsymbol{y} &= \boldsymbol{C_2}\boldsymbol{x} + \boldsymbol{D_{21}}\boldsymbol{w}, \end{aligned} \tag{5.29}$$

where $\hat{\boldsymbol{x}}$ is the estimate of state $\boldsymbol{x}$, and $\hat{\boldsymbol{y}}$ is the estimate of output $\boldsymbol{y}$.

The output estimator $\boldsymbol{L}$, which can regulate the estimated states to the actual states, is designed as

$$\dot{\hat{\boldsymbol{x}}} = \boldsymbol{A}\hat{\boldsymbol{x}} + \boldsymbol{B_2}\boldsymbol{u} + \boldsymbol{L}(\boldsymbol{y} - \hat{\boldsymbol{y}}). \tag{5.30}$$

Then, the system (5.29) can be writen as

$$\begin{aligned} \dot{\hat{\boldsymbol{x}}} &= \boldsymbol{A}\hat{\boldsymbol{x}} + \boldsymbol{B_2}\boldsymbol{u} + \boldsymbol{L}(\boldsymbol{y} - \hat{\boldsymbol{y}}), \\ \hat{\boldsymbol{y}} &= \boldsymbol{C_2}\hat{\boldsymbol{x}}. \end{aligned} \tag{5.31}$$

Note that we do not consider the disturbance $\boldsymbol{w}$ in the estimated output $\hat{\boldsymbol{y}}$. Since $\hat{\boldsymbol{x}}$ is the final estimated state, the output $\hat{\boldsymbol{y}}$ purely relates to the estimated state.

Define $\boldsymbol{e_x} = \boldsymbol{x} - \hat{\boldsymbol{x}}$ as the error between the actual state and the estimated state, and then it implies

$$\begin{aligned} \dot{\boldsymbol{e}}_{\boldsymbol{x}} = \dot{\boldsymbol{x}} - \dot{\hat{\boldsymbol{x}}} &= \boldsymbol{A}\boldsymbol{x} + \boldsymbol{B_1}\boldsymbol{w} + \boldsymbol{B_2}\boldsymbol{u} - \boldsymbol{A}\hat{\boldsymbol{x}} - \boldsymbol{B_2}\boldsymbol{u} + \boldsymbol{L}(\boldsymbol{C_2}\boldsymbol{x} + \boldsymbol{D_{21}}\boldsymbol{w} - \boldsymbol{C_2}\hat{\boldsymbol{x}}) \\ \Rightarrow \quad \dot{\boldsymbol{e}}_{\boldsymbol{x}} &= (\boldsymbol{A} + \boldsymbol{L}\boldsymbol{C_2})\boldsymbol{e_x} + (\boldsymbol{B_1} + \boldsymbol{L}\boldsymbol{D_{21}})\boldsymbol{w}. \end{aligned} \tag{5.32}$$

The error between the real output and the estimated output satisfies

$$\boldsymbol{e_z} = \boldsymbol{z} - \hat{\boldsymbol{y}} = \boldsymbol{C_1}\boldsymbol{x} + \boldsymbol{D_{12}}\boldsymbol{u} - \boldsymbol{C_1}\hat{\boldsymbol{x}} + \boldsymbol{D_{12}}\boldsymbol{u} = \boldsymbol{C_1}\boldsymbol{e_x}. \tag{5.33}$$

Therefore, the closed-loop system (5.29) becomes

$$\begin{aligned} \dot{\boldsymbol{e_x}} &= (\boldsymbol{A} + \boldsymbol{LC_2})\boldsymbol{e_x} + (\boldsymbol{B_1} + \boldsymbol{LD_{21}})\boldsymbol{w}, \\ \boldsymbol{e_z} &= \boldsymbol{C_1}\boldsymbol{e_x}, \end{aligned} \tag{5.34}$$

which can be described as a compact form

$$\boldsymbol{G_f} = \left[\begin{array}{c|c} \boldsymbol{A} + \boldsymbol{LC_2} & \boldsymbol{B_1} + \boldsymbol{LD_{21}} \\ \hline \boldsymbol{C_1} & \boldsymbol{0} \end{array}\right]. \tag{5.35}$$

By (5.4) and (5.6), the objective of the output estimate problem is to minimize the H_2-norm of the transfer function

$$||\boldsymbol{G_f}||_2^2 = \text{Trace}(\boldsymbol{C_1}\boldsymbol{P_c}\boldsymbol{C_1^\top}), \tag{5.36}$$

where $\boldsymbol{P_c}$ satisfies the Lyapunov equation as follows

$$(\boldsymbol{A} + \boldsymbol{LC_2})\boldsymbol{P_c} + \boldsymbol{P_c}(\boldsymbol{A} + \boldsymbol{LC_2})^\top + (\boldsymbol{B_1} + \boldsymbol{LD_{21}})(\boldsymbol{B_1} + \boldsymbol{LD_{21}})^\top = \boldsymbol{0}. \tag{5.37}$$

It implies

$$\boldsymbol{AP_c} + \boldsymbol{P_c}\boldsymbol{A}^\top + \boldsymbol{B_1}\boldsymbol{B_1^\top} + \boldsymbol{LD_{21}}\boldsymbol{D_{21}^\top}\boldsymbol{L}^\top + \boldsymbol{LC_2}\boldsymbol{P_c} + \boldsymbol{P_c}\boldsymbol{C_2^\top}\boldsymbol{L}^\top = \boldsymbol{0}. \tag{5.38}$$

The solution to the output estimation problem is dual to the solution to the full information problem [56].

Define $\boldsymbol{Q_c} = \boldsymbol{B_1}\boldsymbol{B_1^\top}$ and $\boldsymbol{R_c} = \boldsymbol{D_{21}}\boldsymbol{D_{21}^\top}$, and define a full information system as

follows [49]

$$\begin{aligned} \dot{\boldsymbol{x}} &= \boldsymbol{A}^\top \boldsymbol{x} + \boldsymbol{C_1}^\top \boldsymbol{w} + \boldsymbol{C_2}^\top \boldsymbol{u}, \\ \boldsymbol{y} &= \boldsymbol{B_1}^\top \boldsymbol{x} + \boldsymbol{D_{21}}^\top \boldsymbol{u}. \end{aligned} \tag{5.39}$$

By using the results of the full information problem, it is observed that the cost is

$$\text{Trace}(\boldsymbol{C_1 Y_c C_1}^\top), \tag{5.40}$$

where $\boldsymbol{Y_c}$ is the unique symmetric positive solution to the algebraic Riccati equation

$$\boldsymbol{A Y_c} + \boldsymbol{Y_c A}^\top - \boldsymbol{Y_c C_2}^\top \boldsymbol{R_c}^{-1} \boldsymbol{C_2 Y_c} + \boldsymbol{Q_c} = \boldsymbol{0}. \tag{5.41}$$

Let

$$\boldsymbol{L} = -\boldsymbol{Y_2 C_2}^\top \boldsymbol{R_c}^{-1} = -\boldsymbol{Y_2 C_2}^\top (\boldsymbol{D_{21} D_{21}}^\top)^{-1}, \tag{5.42}$$

and then (5.41) is equivalent to (5.37). Since $\boldsymbol{P_c}$ is the unique solution of (5.41), $\boldsymbol{P_c} = \boldsymbol{Y_c}$.

Therefore, the cost of the output estimate H_2 problem is minimized by the estimator

$$\boldsymbol{L} = -\boldsymbol{Y_c C_2}^\top \boldsymbol{R_c}^{-1} = -\boldsymbol{Y_c C_2}^\top (\boldsymbol{D_{21} D_{21}}^\top)^{-1}, \tag{5.43}$$

and the optimal value is obtained by minimizing

$$||\boldsymbol{G_f}||_2^2 = \text{Trace}(\boldsymbol{C_1 Y_2 C_1}^\top), \tag{5.44}$$

where $\boldsymbol{Y_c}$ is the unique solution of the algebraic Riccati equation

$$\boldsymbol{A Y_c} + \boldsymbol{Y_c A}^\top - \boldsymbol{Y_c C_2}^\top (\boldsymbol{D_{21} D_{21}}^\top)^{-1} \boldsymbol{C_2 Y_c} + \boldsymbol{B_1 B_1}^\top = \boldsymbol{0}. \tag{5.45}$$

The estimator in this problem can be considered as a Kalman filter, as it minimizes the error between the real output and estimated output.

5.3.3 State-space Solution to the H_2-optimal Problem

Suppose that the output is finely estimated as states $\hat{\boldsymbol{x}}$, then we can treat the H_2-optimal problem as a full information subproblem. Define $\hat{\boldsymbol{y}}$ is a well known output, then $\hat{\boldsymbol{y}} = \hat{\boldsymbol{x}}$. The full information optimal subsystem can be described as follows

$$\begin{aligned} \dot{\hat{\boldsymbol{x}}} &= \boldsymbol{A}\hat{\boldsymbol{x}} + \boldsymbol{B_1}\boldsymbol{w} + \boldsymbol{B_2}\boldsymbol{u}, \\ \hat{\boldsymbol{z}} &= \boldsymbol{C_1}\hat{\boldsymbol{x}} + \boldsymbol{D_{12}}\boldsymbol{u}, \\ \hat{\boldsymbol{y}} &= \boldsymbol{I}\hat{\boldsymbol{x}}. \end{aligned} \tag{5.46}$$

The compact form of this problem can be expressed as follows

$$\boldsymbol{G_o} = \left[\begin{array}{c|cc} \boldsymbol{A} & \boldsymbol{B_1} & \boldsymbol{B_2} \\ \hline \boldsymbol{C_1} & \boldsymbol{0} & \boldsymbol{D_{12}} \\ \boldsymbol{I} & \boldsymbol{0} & \boldsymbol{0} \end{array}\right]. \tag{5.47}$$

The control gain $\boldsymbol{F}$ can be obtained as

$$\boldsymbol{F} = -(\boldsymbol{D_{12}^\top}\boldsymbol{D_{12}})^{-1}\boldsymbol{B_2^\top}\boldsymbol{X_o}, \tag{5.48}$$

and the control law is

$$\boldsymbol{u} = \boldsymbol{F}\hat{\boldsymbol{y}} = \boldsymbol{F}\hat{\boldsymbol{x}}, \tag{5.49}$$

where $\boldsymbol{X_o}$ is the unique symmetric positive solution to the algebraic Riccati equation

$$\boldsymbol{A}^\top \boldsymbol{X_o} + \boldsymbol{X_o A} - \boldsymbol{X_o B_2}(\boldsymbol{D_{12}^\top D_{12}})^{-1}\boldsymbol{B_2^\top X_o} + \boldsymbol{C_1^\top C_1} = \boldsymbol{0}. \tag{5.50}$$

Since the measured states are the only states we can obtain in the general problem, the error between the measured states and the estimated states should be considered. An output optimal subproblem can be designed to solve this problem. Define an input $\boldsymbol{v}$ as the difference between the real control input $\boldsymbol{u}$ and the estimated input, $\boldsymbol{v} = \boldsymbol{F\hat{x}} - \boldsymbol{Fx} = \boldsymbol{u} - \boldsymbol{Fx}$. Consider $\boldsymbol{v}$ as a new control input, and then the general problem becomes an output estimation optimal subproblem as follows

$$\begin{aligned} \dot{\boldsymbol{x}} &= \boldsymbol{Ax} + \boldsymbol{B_1 w} + \boldsymbol{B_2 u}, \\ \boldsymbol{v} &= -\boldsymbol{Fx} + \boldsymbol{Iu}, \\ \boldsymbol{y} &= \boldsymbol{C_2 x} + \boldsymbol{D_{21} w}. \end{aligned} \tag{5.51}$$

The form of this output estimation problem can also be expressed as follows

$$\boldsymbol{G_c} = \left[\begin{array}{c|cc} \boldsymbol{A} & \boldsymbol{B_1} & \boldsymbol{B_2} \\ \hline -\boldsymbol{F} & \boldsymbol{0} & \boldsymbol{I} \\ \boldsymbol{C_2} & \boldsymbol{D_{21}} & \boldsymbol{0} \end{array}\right]. \tag{5.52}$$

Based on the results for the output estimation problem, the estimator L gain can be obtained as

$$\boldsymbol{L} = -\boldsymbol{Y_c C_2^\top}(\boldsymbol{D_{21} D_{21}^\top})^{-1}, \tag{5.53}$$

where $\boldsymbol{Y_c}$ is the unique solution of the algebraic Riccati equation

$$\boldsymbol{AY_c} + \boldsymbol{Y_c A^\top} - \boldsymbol{Y_c C_2^\top}(\boldsymbol{D_{21} D_{21}^\top})^{-1}\boldsymbol{C_2 Y_c} + \boldsymbol{B_1 B_1^\top} = \boldsymbol{0}. \tag{5.54}$$

This estimator can minimize the difference between the estimated state and the actual state, and therefore it regulate the estimated output to the actual output [57].

By minimizing the effect from disturbance $\boldsymbol{w}$ to the estimated output $\hat{\boldsymbol{z}}$ and minimizing the difference between the estimated output $\hat{\boldsymbol{z}}$ and the actual output $\boldsymbol{z}$, the controller $\boldsymbol{K}$ is finally developed for the following general H_2-optimal problem

$$\begin{aligned} \dot{\hat{\boldsymbol{x}}} &= \boldsymbol{A}\hat{\boldsymbol{x}} + \boldsymbol{B_2}\boldsymbol{u} + \boldsymbol{L}(\boldsymbol{C_2}\hat{\boldsymbol{x}} - \boldsymbol{y}), \\ \boldsymbol{u} &= \boldsymbol{F}\hat{\boldsymbol{x}}. \end{aligned} \tag{5.55}$$

Rewrite the $\boldsymbol{K}$ as a state-space form

$$\begin{aligned} \dot{\boldsymbol{x}}_{\boldsymbol{k}} &= \boldsymbol{A}_{\boldsymbol{k}}\boldsymbol{x}_{\boldsymbol{k}} + \boldsymbol{B}_{\boldsymbol{k}}\boldsymbol{y}, \\ \boldsymbol{u} &= \boldsymbol{C}_{\boldsymbol{k}}\boldsymbol{x}_{\boldsymbol{k}} + \boldsymbol{D}_{\boldsymbol{k}}\boldsymbol{y}, \end{aligned} \tag{5.56}$$

where

$$\boldsymbol{A}_{\boldsymbol{k}} = \boldsymbol{A} + \boldsymbol{L}\boldsymbol{C_2} + \boldsymbol{B_2}\boldsymbol{F}, \quad \boldsymbol{B}_{\boldsymbol{k}} = \boldsymbol{L}, \quad \boldsymbol{C}_{\boldsymbol{k}} = -\boldsymbol{F}, \quad \boldsymbol{D}_{\boldsymbol{k}} = \boldsymbol{0}. \tag{5.57}$$

The controller $\boldsymbol{K}$ can also be expressed as

$$\boldsymbol{K} = \left[\begin{array}{c|c} \boldsymbol{A} + \boldsymbol{L}\boldsymbol{C_2} + \boldsymbol{B_2}\boldsymbol{F} & \boldsymbol{L} \\ \hline -\boldsymbol{F} & \boldsymbol{0} \end{array}\right], \tag{5.58}$$

where $\boldsymbol{F}$ and $\boldsymbol{L}$ are with the following definition

$$\begin{aligned} \boldsymbol{F} &= -(\boldsymbol{D}_{\boldsymbol{12}}^{\top}\boldsymbol{D_{12}})^{-1}\boldsymbol{B}_{\boldsymbol{2}}^{\top}\boldsymbol{X_o} \\ \boldsymbol{L} &= -\boldsymbol{Y_c}\boldsymbol{C}_{\boldsymbol{2}}^{\top}(\boldsymbol{D_{21}}\boldsymbol{D}_{\boldsymbol{21}}^{\top})^{-1}, \end{aligned} \tag{5.59}$$

and $\boldsymbol{X_o}$ and $\boldsymbol{Y_c}$ are the unique symmetric positive solutions of the following algebraic

Riccati equations, respectively.

$$\begin{aligned} \boldsymbol{A}^\top \boldsymbol{X_o} + \boldsymbol{X_o A} - \boldsymbol{X_o B_2}(\boldsymbol{D_{12}^\top D_{12}})^{-1}\boldsymbol{B_2^\top X_o} + \boldsymbol{C_1^\top C_1} = \boldsymbol{0}, \\ \boldsymbol{A Y_c} + \boldsymbol{Y_c A}^\top - \boldsymbol{Y_c C_2^\top}(\boldsymbol{D_{21} D_{21}^\top})^{-1}\boldsymbol{C_2 Y_c} + \boldsymbol{B_1 B_1^\top} = \boldsymbol{0}. \end{aligned} \tag{5.60}$$

The closed-loop system is formulated as

$$\begin{aligned} \dot{\boldsymbol{x}}_{\boldsymbol{cl}} &= \boldsymbol{A_{cl}}\boldsymbol{x_{cl}} + \boldsymbol{B_{cl}}\boldsymbol{w} \\ \boldsymbol{z} &= \boldsymbol{C_{cl}}\boldsymbol{x_{cl}} + \boldsymbol{D_{cl}}\boldsymbol{w}, \end{aligned} \tag{5.61}$$

where

$$\begin{aligned} \boldsymbol{x_{cl}} &= \begin{bmatrix} \boldsymbol{x} \\ \boldsymbol{x_k} \end{bmatrix} \\ \boldsymbol{A_{cl}} &= \begin{bmatrix} \boldsymbol{A} + \boldsymbol{B_2 D_k C_2} & \boldsymbol{B_2 C_k} \\ \boldsymbol{B_k C_2} & \boldsymbol{A_k} \end{bmatrix} \\ \boldsymbol{B_{cl}} &= \begin{bmatrix} \boldsymbol{B_1} + \boldsymbol{B_2 D_k D_{21}} \\ \boldsymbol{B_k D_{21}} \end{bmatrix} \\ \boldsymbol{C_{cl}} &= \begin{bmatrix} \boldsymbol{C_1} + \boldsymbol{D_{12} D_k C_2} & \boldsymbol{D_{12} C_k} \end{bmatrix} \\ \boldsymbol{D_{cl}} &= \boldsymbol{D_{11}} + \boldsymbol{D_{12} D_k D_{21}}. \end{aligned} \tag{5.62}$$

5.4 LMI Solution to the H_2-optimal Control Problem

The state-space method for solving the H_2-optimal problem is convenient to follow. However, the formulation of the model with all assumptions is difficult. Therefore, we reduce the H_2-optimal problem to an LMI problem. The LMI method is a tool to

design the controllers in terms of linear matrix inequalities with a few assumptions [40], and LMIs can be conveniently solved by using the existing standard LMI solvers in MATLAB. Therefore, the application process of the LMI method is simpler than that of the state-space approach.

5.4.1 Basic Concepts of the LMI Approach

A system of LMIs is a set of matrix inequalities with the following common form

$$\boldsymbol{F_L} = \boldsymbol{F_0} + \sum_{i=1}^{n} x_i \boldsymbol{F_i} \succeq 0, \tag{5.63}$$

where $\boldsymbol{F_i} \in \mathbb{R}^{s \times s}$ $(i = 1, 2, ...n)$ are symmetric matrices, x_i $(i = 1, 2, ...n)$ are unknown scalar variables [58], and the inequality symbol $\succeq$ means that the matrix in the left side is positive semidefinite.

We now introduce the Schur complement which is usually used for the derivation of the general LMI problems. It shows that the set of nonlinear inequalities

$$\begin{aligned} \boldsymbol{M} &\succ 0 \\ \boldsymbol{Q} - \boldsymbol{R}^\top \boldsymbol{M}^{-1} \boldsymbol{R} &\succ 0, \end{aligned} \tag{5.64}$$

or

$$\begin{aligned} \boldsymbol{Q} &\succ 0 \\ \boldsymbol{M} - \boldsymbol{R}\boldsymbol{Q}^{-1} \boldsymbol{R}^\top &\succ 0, \end{aligned} \tag{5.65}$$

can be equivalently represented as the LMI as follows

$$\begin{bmatrix} \boldsymbol{M} & \boldsymbol{R} \\ \boldsymbol{R}^\top & \boldsymbol{Q} \end{bmatrix} \succ 0, \tag{5.66}$$

where $\boldsymbol{M} \in \mathbb{R}^{p\times p}$ and $\boldsymbol{Q} \in \mathbb{R}^{q\times q}$ are symmetric matrices, $\boldsymbol{R} \in \mathbb{R}^{p\times q}$, and the inequality symbol $\succ$ means that the matrix in the left side is positive definite [40].

Using (5.3-5.6), it is readily verified that the H_2-norm $||\boldsymbol{T_o}||_2^2 < \alpha$ if there exists a positive $\boldsymbol{P_c}$ satisfying [59]

$$\begin{aligned} \text{Trace}(\boldsymbol{C_o P_c C_o^\top}) &< \alpha \\ \boldsymbol{A_o P_c} + \boldsymbol{P_c A_o^\top} + \boldsymbol{B_o B_o^\top} &\prec 0 \end{aligned} \tag{5.67}$$

or there exists a positive $\boldsymbol{P_o}$ satisfying

$$\begin{aligned} \text{Trace}(\boldsymbol{B_o^\top P_o B_o}) &< \alpha \\ \boldsymbol{A_o^\top P_o} + \boldsymbol{P_o A_o} + \boldsymbol{C_o^\top C_o} &\prec 0. \end{aligned} \tag{5.68}$$

In other words, the Lyapunov inequalities on $\boldsymbol{P_c}$ and $\boldsymbol{P_o}$ are the special forms of LMIs [60].

Via the Schur complement, the matrix inequality (5.67) and (5.68) can be transformed to the LMI standard expressions [61]

$$\begin{aligned} \text{Trace}(\boldsymbol{Z_c}) &< \alpha \\ \begin{bmatrix} \boldsymbol{P_c} & \boldsymbol{B_o} \\ \boldsymbol{B_o^\top} & \boldsymbol{Z_c} \end{bmatrix} &\succ 0 \\ \begin{bmatrix} \boldsymbol{A_o P_c} + \boldsymbol{P_c A_o^\top} & \boldsymbol{P_c C_o^\top} \\ \boldsymbol{C_o P_c} & -\boldsymbol{I_r} \end{bmatrix} &\prec 0, \end{aligned} \tag{5.69}$$

and

$$\begin{aligned} \text{Trace}(\boldsymbol{Z_o}) &< \alpha \\ \begin{bmatrix} \boldsymbol{P_o} & \boldsymbol{C_o^\top} \\ \boldsymbol{C_o} & \boldsymbol{Z_o} \end{bmatrix} &\succ 0 \\ \begin{bmatrix} \boldsymbol{A_o^\top P_o + P_o A_o} & \boldsymbol{P_o B_o} \\ \boldsymbol{B_o^\top P_o} & \boldsymbol{-I_r} \end{bmatrix} &\prec 0 \end{aligned} \tag{5.70}$$

by setting $\boldsymbol{P_o} = \boldsymbol{P_c^{-1}}$ [62], where $\boldsymbol{I_r}$ is identity matrix.

5.4.2 LMI Solution to the H_2-optimal Control Problem

Considering the closed-loop system (5.61), the H_2-norm of cost function $||\boldsymbol{T_{zw}}||_2^2$ is less than α if and only if there exists positive $\boldsymbol{P_{cl}}$ satisfying

$$\begin{aligned} \text{Trace}(\boldsymbol{W_L}) &< \alpha \\ \begin{bmatrix} \boldsymbol{P_{cl}} & \boldsymbol{B_{cl}} \\ \boldsymbol{B_{cl}^\top} & \boldsymbol{W_L} \end{bmatrix} &\succ 0 \\ \begin{bmatrix} \boldsymbol{A_{cl} P_{cl} + P_{cl} A_{cl}^\top} & \boldsymbol{P_{cl} C_{cl}^\top} \\ \boldsymbol{C_{cl} P_{cl}} & \boldsymbol{-I_r} \end{bmatrix} &\prec 0 \end{aligned} \tag{5.71}$$

and

$$\boldsymbol{D_{cl}} = \boldsymbol{0}. \tag{5.72}$$

The LMIs (5.71) can be simplified through a specific change of variables [60].

Partition $\boldsymbol{P_{cl}}$ and $\boldsymbol{P_{cl}^{-1}}$ as follows

$$\boldsymbol{P_{cl}} = \begin{bmatrix} \boldsymbol{P_L} & \bar{\boldsymbol{P}}_{\boldsymbol{L}}^{\top} \\ \bar{\boldsymbol{P}}_{\boldsymbol{L}} & \times \end{bmatrix}, \qquad \boldsymbol{P_{cl}^{-1}} = \begin{bmatrix} \boldsymbol{Q_L} & \bar{\boldsymbol{Q}}_{\boldsymbol{L}} \\ \bar{\boldsymbol{Q}}_{\boldsymbol{L}}^{\top} & \times \end{bmatrix}, \tag{5.73}$$

where $\times$ denotes the block which we do not care in the results, and $\bar{\boldsymbol{P}}_{\boldsymbol{L}}$ and $\bar{\boldsymbol{Q}}_{\boldsymbol{L}}$ can be obtained from $\boldsymbol{P_L}$ and $\boldsymbol{Q_L}$ based on the relationship as follows

$$\boldsymbol{P_L Q_L} + \bar{\boldsymbol{P}}_{\boldsymbol{L}} \bar{\boldsymbol{Q}}_{\boldsymbol{L}} = \mathbf{1}. \tag{5.74}$$

Define four variables $\boldsymbol{X_L}$, $\boldsymbol{Y_L}$, $\boldsymbol{U_L}$, and $\boldsymbol{V_L}$ that have the following relationship

$$\begin{bmatrix} \boldsymbol{X_L} & \boldsymbol{U_L} \\ \boldsymbol{Y_L} & \boldsymbol{V_L} \end{bmatrix} = \begin{bmatrix} \bar{\boldsymbol{P}}_{\boldsymbol{L}} & \boldsymbol{P_L B_L} \\ \mathbf{0} & \boldsymbol{I} \end{bmatrix} \begin{bmatrix} \boldsymbol{A_k} & \boldsymbol{B_k} \\ \boldsymbol{C_k} & \boldsymbol{D_k} \end{bmatrix} \begin{bmatrix} \bar{\boldsymbol{Q}}_{\boldsymbol{L}} & \mathbf{0} \\ \boldsymbol{C_L Q_L} & \boldsymbol{I} \end{bmatrix} + \begin{bmatrix} \boldsymbol{P_L} \\ \mathbf{0} \end{bmatrix} \boldsymbol{A} \begin{bmatrix} \boldsymbol{Q_L} & \mathbf{0} \end{bmatrix}. \tag{5.75}$$

It implies

$$\begin{bmatrix} \boldsymbol{A_k} & \boldsymbol{B_k} \\ \boldsymbol{C_k} & \boldsymbol{D_k} \end{bmatrix} = \begin{bmatrix} \bar{\boldsymbol{P}}_{\boldsymbol{L}}^{-1} & -\bar{\boldsymbol{P}}_{\boldsymbol{L}}^{-1} \boldsymbol{P_L B_L} \\ \mathbf{0} & \boldsymbol{I} \end{bmatrix} \begin{bmatrix} \boldsymbol{X_L} - \boldsymbol{P_L A Q_L} & \boldsymbol{U_L} \\ \boldsymbol{Y_L} & \boldsymbol{V_L} \end{bmatrix} \begin{bmatrix} \bar{\boldsymbol{Q}}_{\boldsymbol{L}}^{-1} & \mathbf{0} \\ -\boldsymbol{C_L Q_L} \bar{\boldsymbol{Q}}_{\boldsymbol{L}}^{-1} & \boldsymbol{I} \end{bmatrix}. \tag{5.76}$$

The LMI for the general H_2-optimal problem therefore is derived as follows

$$
\begin{aligned}
&\mathrm{Trace}(\boldsymbol{W_L}) < \alpha \\
&\boldsymbol{D_{11}} + \boldsymbol{D_{12}} \boldsymbol{V_L} \boldsymbol{D_{21}} = \boldsymbol{0} \\
&\begin{bmatrix} \boldsymbol{W_L} & \boldsymbol{C_1 Q_L} + \boldsymbol{D_{12}} \boldsymbol{Y_L} & \boldsymbol{C_1} + \boldsymbol{D_{12}} \boldsymbol{V_L} \boldsymbol{C_2} \\ \star & \boldsymbol{Q_L} & \boldsymbol{I} \\ \star & \star & \boldsymbol{P_L} \end{bmatrix} \succ 0 \\
&\begin{bmatrix} \boldsymbol{A Q_L} + \boldsymbol{B_2 Y_L} + (\boldsymbol{A Q_L} + \boldsymbol{B_2 Y_L})^\top & \boldsymbol{A} + \boldsymbol{B_2} \boldsymbol{V_L} \boldsymbol{C_2} + \boldsymbol{X_L}^\top & \boldsymbol{B_1} + \boldsymbol{B_2} \boldsymbol{V_L} \boldsymbol{D_{21}} \\ \star & \boldsymbol{P_L A} + \boldsymbol{U_L C_2} + (\boldsymbol{P_L A} + \boldsymbol{U_L C_2})^\top & \boldsymbol{P_L B_1} + \boldsymbol{U_L D_{21}} \\ \star & \star & -\boldsymbol{I} \end{bmatrix} \prec 0,
\end{aligned}
\tag{5.77}
$$

where $\star$ means the matrix transpose of the symmetrical element in the matrix. $\boldsymbol{Q_L}$, $\boldsymbol{P_L}$, and $\boldsymbol{W_L}$ are the decision variables from Lyapunov inequality, while $\boldsymbol{X_L}$, $\boldsymbol{Y_L}$, $\boldsymbol{U_L}$, and $\boldsymbol{V_L}$ are the decision matrices from the H_2-optimal controller.

By (5.76), the controller can be achieved by

$$
\begin{aligned}
\boldsymbol{M_L} =& \boldsymbol{Q_L P_L} - \boldsymbol{I}, \\
\boldsymbol{N_L} =& \boldsymbol{M_L}^{-1}((\boldsymbol{A Q_L} + \boldsymbol{B_2 Y_L}) + \boldsymbol{Q_L}(\boldsymbol{A} + \boldsymbol{B_2} \boldsymbol{D_K} \boldsymbol{C_2})^\top, \\
& + \boldsymbol{Q_L}(\boldsymbol{C_1} + \boldsymbol{D_{12}} \boldsymbol{D_K} \boldsymbol{C_2})^\top (\boldsymbol{C_1 Q_L} + \boldsymbol{D_{12}} \boldsymbol{Y_L})) \boldsymbol{Q_L}^{-1}, \\
\boldsymbol{D_k} =& \boldsymbol{V_L}, \\
\boldsymbol{C_k} =& -\boldsymbol{D_k C_2} + \boldsymbol{Y_L} \boldsymbol{Q_L}^{-1}, \\
\boldsymbol{B_k} =& \boldsymbol{B_2 D_k} - \boldsymbol{M_L}^{-1}(\boldsymbol{Q_L U_L} - \boldsymbol{B_2 D_k}), \\
\boldsymbol{A_k} =& \boldsymbol{A} + \boldsymbol{B_2 D_k C_2} + \boldsymbol{B_2 C_k} - \boldsymbol{B_k C_2} + \boldsymbol{N_L}.
\end{aligned}
\tag{5.78}
$$

5.5 H_2-optimal Controller Design for the Position Subsystem of the Quadrotor

5.5.1 Simulation Setup

Assume that the system in (3.32) is affected by an external disturbances $\boldsymbol{W_1 y_{w1}}$, e.g., wind disturbance, a bounded model uncertainty $\boldsymbol{U_2 u_\theta}$, and a bounded measurement uncertainty $\boldsymbol{W_2 w_2}$, as shown in Figure 5.1.

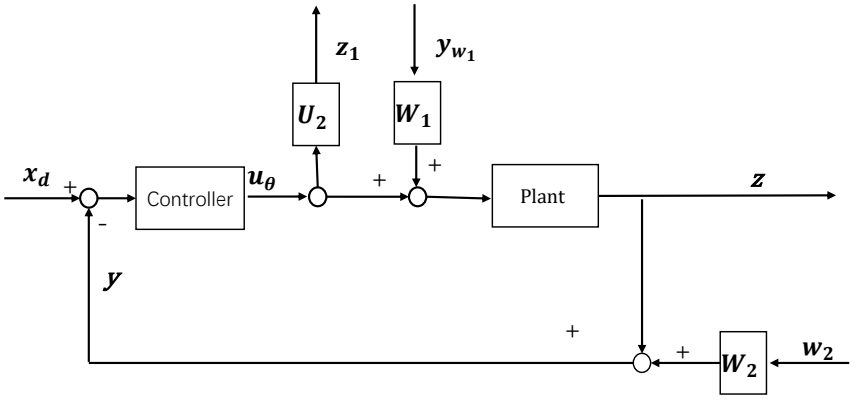

Figure 5.1: Plant with disturbances and uncertainties.

Assume that only two states can be measured. The plant (3.32) is augmented as follows

$$\begin{aligned} \dot{\boldsymbol{x}} &= \boldsymbol{A x} + \boldsymbol{W_1 y_{w1}} + \boldsymbol{B_2 u_\theta}, \\ \boldsymbol{z} &= \boldsymbol{C_1 x}, \\ \boldsymbol{z_1} &= \boldsymbol{U_2 u_\theta}, \\ \boldsymbol{y} &= \boldsymbol{C_2 x} + \boldsymbol{W_2 w_2}, \end{aligned} \tag{5.79}$$

where

$$\boldsymbol{A} = \boldsymbol{A_X},\ \boldsymbol{B_2} = \boldsymbol{B_X},\ \boldsymbol{C_1} = \begin{bmatrix} 1 & 0 & 0 & 0 & 0 \end{bmatrix},\ \boldsymbol{C_2} = \begin{bmatrix} 1 & 0 & 0 & 0 & 0 \\ 0 & 0 & 0 & 0 & 0 \\ 0 & 0 & 1 & 0 & 0 \\ 0 & 0 & 0 & 0 & 0 \\ 0 & 0 & 0 & 0 & 0 \end{bmatrix}.$$

Suppose that the external disturbance is generated by a general model as follows

$$\begin{aligned} \dot{\boldsymbol{x}}_{\boldsymbol{w1}} &= \boldsymbol{A}_{\boldsymbol{w1}}\boldsymbol{x}_{\boldsymbol{w1}} + \boldsymbol{B}_{\boldsymbol{w1}}\boldsymbol{w}_{\boldsymbol{1}}, \\ \boldsymbol{y}_{\boldsymbol{w1}} &= \boldsymbol{C}_{\boldsymbol{w1}}\boldsymbol{x}_{\boldsymbol{w1}}, \end{aligned} \tag{5.80}$$

where

$$\boldsymbol{A}_{\boldsymbol{w1}} = -0.2,\ \boldsymbol{B}_{\boldsymbol{w1}} = 0.6,\ \boldsymbol{C}_{\boldsymbol{w1}} = 1,$$

and $\boldsymbol{w_1}$ is white Gaussian noise with equal intensity for all frequencies [55].

Then, the plant (5.79) is augmented to a state-space model as follows

$$\begin{aligned} \dot{\boldsymbol{x}}_{\boldsymbol{a}} &= \boldsymbol{A}_{\boldsymbol{a}}\boldsymbol{x}_{\boldsymbol{a}} + \boldsymbol{B}_{\boldsymbol{1a}}\boldsymbol{w}_{\boldsymbol{a}} + \boldsymbol{B}_{\boldsymbol{2a}}\boldsymbol{u}_{\boldsymbol{\theta}}, \\ \boldsymbol{z}_{\boldsymbol{a}} &= \boldsymbol{C}_{\boldsymbol{1a}}\boldsymbol{x}_{\boldsymbol{a}} + \boldsymbol{D}_{\boldsymbol{11a}}\boldsymbol{w}_{\boldsymbol{a}} + \boldsymbol{D}_{\boldsymbol{12a}}\boldsymbol{u}_{\boldsymbol{\theta}}, \\ \boldsymbol{y}_{\boldsymbol{a}} &= \boldsymbol{C}_{\boldsymbol{2a}}\boldsymbol{x}_{\boldsymbol{a}} + \boldsymbol{D}_{\boldsymbol{21a}}\boldsymbol{w}_{\boldsymbol{a}}, \end{aligned} \tag{5.81}$$

where

$$
\begin{aligned}
\boldsymbol{x_a} &= \begin{bmatrix} \boldsymbol{x} \\ \boldsymbol{x_{w1}} \end{bmatrix}, \boldsymbol{z_a} = \begin{bmatrix} \boldsymbol{z} \\ \boldsymbol{z_1} \end{bmatrix}, \boldsymbol{y_a} = \boldsymbol{y}, \boldsymbol{w_a} = \begin{bmatrix} \boldsymbol{w_1} \\ \boldsymbol{w_2} \end{bmatrix}, \\
\boldsymbol{A_a} &= \begin{bmatrix} \boldsymbol{A} & \boldsymbol{W_1 C_{w1}} \\ \boldsymbol{0} & \boldsymbol{A_{w1}} \end{bmatrix}, \boldsymbol{B_{1a}} = \begin{bmatrix} \boldsymbol{0} & \boldsymbol{0} \\ \boldsymbol{B_{w1}} & \boldsymbol{0} \end{bmatrix}, \boldsymbol{B_{2a}} = \begin{bmatrix} \boldsymbol{B_2} \\ \boldsymbol{0} \end{bmatrix}, \\
\boldsymbol{C_{1a}} &= \begin{bmatrix} \boldsymbol{C_1} & \boldsymbol{0} \\ \boldsymbol{0} & \boldsymbol{0} \end{bmatrix}, \boldsymbol{D_{11a}} = \begin{bmatrix} \boldsymbol{0} & \boldsymbol{0} \\ \boldsymbol{0} & \boldsymbol{0} \end{bmatrix}, \boldsymbol{D_{12a}} = \begin{bmatrix} \boldsymbol{0} \\ \boldsymbol{U_2} \end{bmatrix}, \\
\boldsymbol{C_{2a}} &= \begin{bmatrix} \boldsymbol{C_2} & \boldsymbol{0} \end{bmatrix}, \boldsymbol{D_{21a}} = \begin{bmatrix} \boldsymbol{0} & \boldsymbol{W_2} \end{bmatrix}.
\end{aligned} \tag{5.82}
$$

This augmented system has the same form as (5.7). Suppose that the initial state of the quadrotor $\boldsymbol{x_0}$ is $[0.5, 0, 0, 0, 0]^\top$, and the desired state is $[0, 0, 0, 0, 0]^\top$. It is assumed that

$$
\boldsymbol{W_1} = \begin{bmatrix} 0 & 0.0198 & 0 & 0.011 & 0 \end{bmatrix}^\top, \ \boldsymbol{W_2} = 0.01\boldsymbol{I_5}, \ \boldsymbol{U_2} = 0.01, \tag{5.83}
$$

where $\boldsymbol{I_5}$ is the identity matrix.

5.5.2 Simulation Results

Figure 5.2 shows the trajectories of the states and the control input. Since the LQR controller can not be implemented without the full state measurement, the LQR controller here is adopted to control a nominal model with the full state information. The H_2-optimal controller is designed to account for the uncertainties and disturbances in the system with partial states. It is verified that the H_2-optimal controller can stabilize the position of the quadrotor, despite the presence of bounded disturbances and uncertainties.

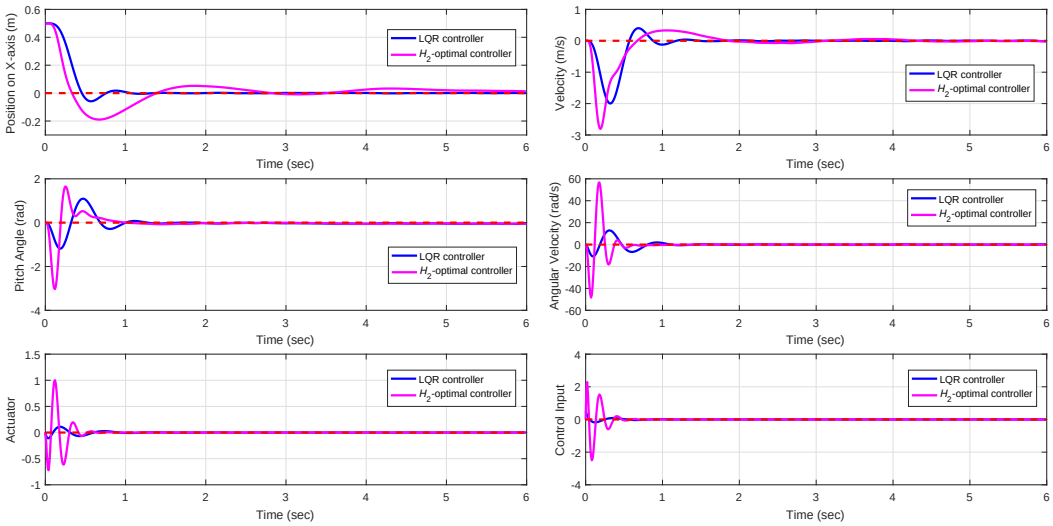

Figure 5.2: Simulation results of the state feedback H_2-optimal controller.

The simulation study is given to explore the effects of disturbances and uncertainties with varying values of the parameters. One result is that the value of the measurement uncertainty affects the output. Figure 5.3 shows that the controller performance changes under different magnitudes of measurement uncertainties. A large value of $\boldsymbol{W_2}$ means that the measurement implies a lot of noise, and then the controller stabilizes the quadrotor slower.

Another result is that the magnitude of $\boldsymbol{W_1}$ determines the amount of affecting of the external disturbances. Figure 5.4 shows the comparative result of the disturbance $\boldsymbol{W_1}$ with different magnitudes. A larger magnitude of $\boldsymbol{W_1}$ causes a faster response.

The third result is that the model uncertainty takes a smaller influence over the plant compared with the external disturbance and the measurement uncertainty. Figure 5.5 shows that the performance of the controller does not change much under the different values of $\boldsymbol{U_2}$.

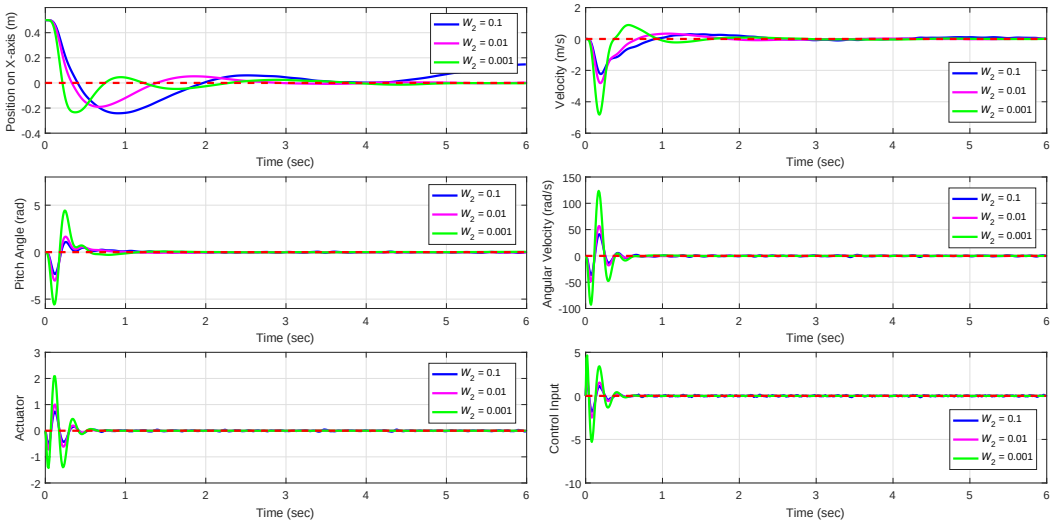

Figure 5.3: Simulation results under different values of measurement uncertainties.

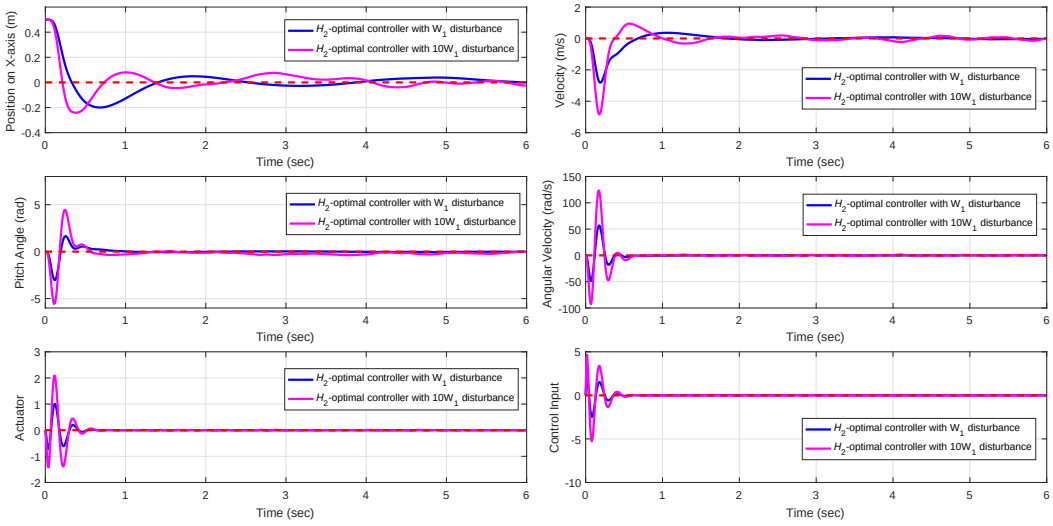

Figure 5.4: Simulation results under different magnitudes of disturbances.

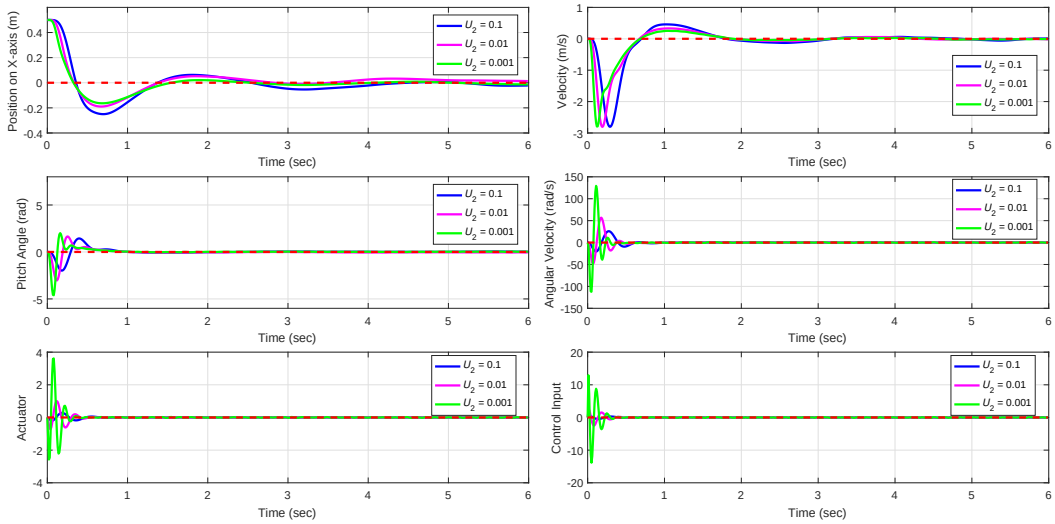

Figure 5.5: Simulation results under different values of model uncertainties.

5.6 Experiments

This section describes the implementation of the H_2-optimal controller for a quadrotor in the presence of disturbances and uncertainties. As shown in Figure 5.6, the indoor quadrotor is experimentally tested using an inner-outer loop control structure: an inner loop for attitude control and an outer loop for altitude and position control.

A cascaded controller is used for this quadrotor system. In the outer loop, a PID controller and an LQR controller are adopted for the altitude and position control, respectively. In the inner loop, a PD controller and the proposed H_2-optimal controller are applied in the yaw angle control and pitch and roll angel control, respectively. The X-position and Y-position are incorporated in the H_2-optimal controller in the inner loop, and the disturbances and the uncertainties also affect the system in the inner loop. We then focus on the performance of the H_2-optimal controllers in the X and Y-position. In the XY-plane, the state feedback H_2-optimal controller is applied for the waypoint tracking. The desired waypoint tracking task is as follows. First, the quadrotor is operated to the point $[0.3, 0.3]^\top$. Then, the quadrotor hovers

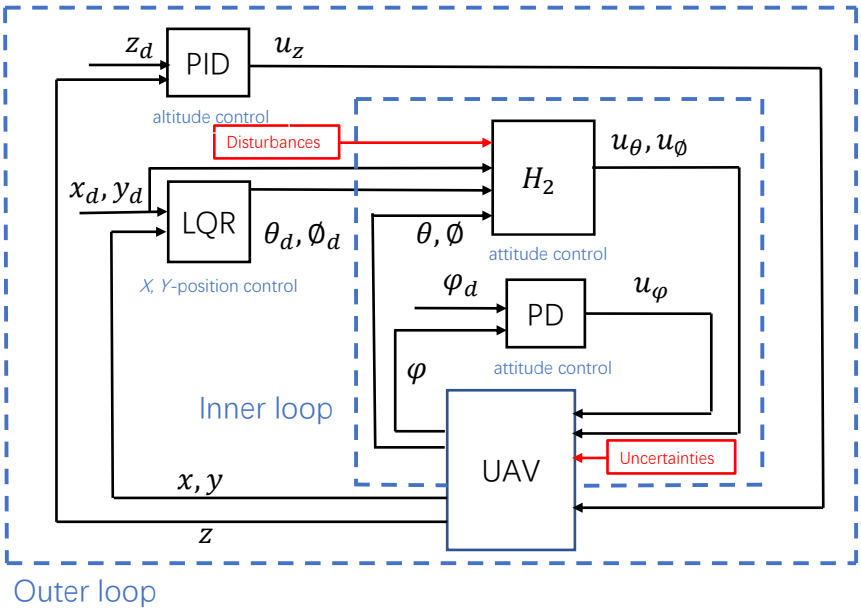

Figure 5.6: Inner-outer loop control structure.

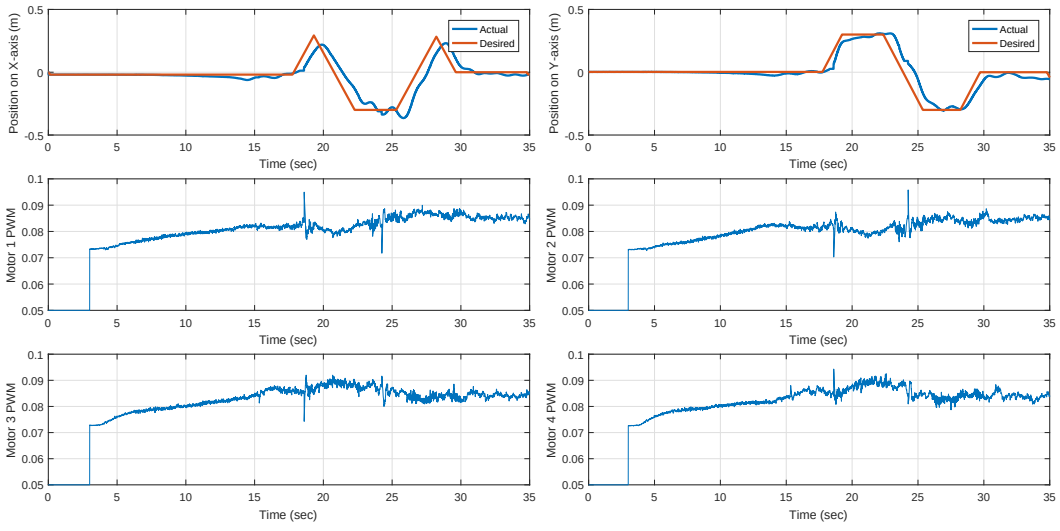

Figure 5.7: Experimental results: Time response of the positions and the PWM signals.

sequentially at $[-0.3, 0.3]^\top$, $[-0.3, -0.3]^\top$, $[0.3, -0.3]^\top$. Finally, the quadrotor comes back at the original point. Figure 5.7 shows the X and Y positions of the quadrotor for the experimental test. The model uncertainty and measurement uncertainty are added to the quadrotor dynamics, and the wind disturbances are also brought to the system. It is verified that the H_2-optimal controller can regulate the quadrotor to the desired position with the attendance of disturbances and uncertainties.

5.7 Conclusion

This chapter provides the solutions to the H_2-optimal problem. The solutions are obtained via the state-space approach and the LMI method, respectively. A state feedback H_2-optimal controller is designed for the X-position subsystem of the quadorotor. The simulation results and the experimental results are presented and analyzed in detail, showing that the proposed H_2-optimal controller can be employed to reject the disturbances and uncertainties.

Chapter 6

Conclusion and Future Work

6.1 Conclusion

The work in this thesis focuses on the introduction of the experimental platform and the system dynamics of the quadrotor. The experimental system includes a ground station, a quadrotor, and a motion capture system. In terms of the system dynamics, Euler-Lagrange approach is employed step by step to derive the dynamic model. After the combination of the quadrotor dynamic model and the actuator dynamic model, a state-space dynamic model is provided for further research.

Two types of control methods for the quadrotor, including LQR control methods and H_2-optimal control methods, are studied in this thesis. The simulation results are compared.

LQR control methods are discussed for a nominal model. From the simulation results, the controllers are verified that it can stabilize the quadrotor and operate the quadrotor from the initial position to the desired position steadily.

In order to decrease the influence of exogenous disturbances and uncertainties, the H_2-optimal controller is provided. First, the state-space approach of the H_2-optimal

control methods is derived. Different from the LQR control method, the H_2-optimal control method consists of the LQR controller for the full information problem and the LQE controller for the output estimation problem. The controller is obtained by solving Riccati equations. Next, the solution of H_2-optimal problem is studied via the LMI approach. The state feedback H_2-optimal controller for the position subsystem of the quadrotor is simulated and tested on the experimental system at the end. The state feedback H_2-optimal controller shows a good system performance to avoid the disturbances and uncertainties.

6.2 Future Work

Based on the researches provided in this thesis, some explorations are expected in the future.

The H_2-optimal controller works better for the system with disturbances and uncertainties if it is applied together with other control methods, for example, H_∞ control. The maximum values of the disturbances can be estimated. The design of mixed H_2-optimal and H_∞ controller and the comparison with the state feedback H_2-optimal controller can be used as ideas for the further research.

The H_2-optimal controller employed in this thesis is not only used to stabilize the system but also to force the quadrotor system to track the desired reference trajectory, even under the attendance of the disturbances and uncertainties. It means that the H_2-optimal controller will be suitable for more general experimental situations. However, it is difficult to build an experimental system to simulate these general situations due to the complex disturbance models. Designing a system to simulate the general experimental situations and developing an H_2-optimal controller to regulate the quadrotor in this general experimental system are worth more attention in the

further work.

All of the proposed controllers in this thesis are based on the continuous-time system. However, in practical applications, the control systems are operated in sampled-data models. In our previous work, the continuous-time controllers can be converted to the discrete-time one automatically by the simulation tool in the experimental system, yet some approximation errors will occur in the process of discretization [50]. Therefore, another future work will focus on obtaining and comparing the discrete-time controllers via different discretization techniques and verifying these controllers in the experimental system.

Bibliography

[1] Kunwu Zhang. Flight Control of a Quadrotor: Theory and Experiments. Master's thesis, 2016.

[2] *Quanser QBall-X4 User Manual*. Quanser Consulting Inc., Markham, Ontario, Canada, 2010.

[3] Arthur Holland Michel, Dan Gettinger, and H Michel. Drone year in review: 2017. *Center for the Study of the Drone at Bard College*, 2018.

[4] Anuj Puri. A survey of unmanned aerial vehicles (UAV) for traffic surveillance. *Department of computer science and engineering, University of South Florida*, pages 1–29, 2005.

[5] Xiaohua Tong, Xiangfeng Liu, Peng Chen, Shijie Liu, Kuifeng Luan, Lingyun Li, Shuang Liu, Xianglei Liu, Huan Xie, Yanmin Jin, et al. Integration of UAV-based photogrammetry and terrestrial laser scanning for the three-dimensional mapping and monitoring of open-pit mine areas. *Remote Sensing*, 7(6):6635–6662, 2015.

[6] Connie Phan and Hugh HT Liu. A cooperative UAV/UGV platform for wildfire detection and fighting. In *Proceedings of Asia Simulation Conference-7th International Conference on System Simulation and Scientific Computing*, pages 494–498, Beijing, China, Oct. 2008. IEEE.

[7] D Giles and R Billing. Deployment and performance of a UAV for crop spraying. *Chemical Engineering Transactions*, 44:307–312, 2015.

[8] Konstantinos Dalamagkidis. Classification of UAVs. *Handbook of Unmanned Aerial Vehicles*, pages 83–91, 2015.

[9] Ruth Tesfaye. Modeling and Control of a Quad-rotor Unmanned Aerial Vehicle at Hovering Position. *Addis Ababa University, School of Graduate Studies, Addis Ababa Institute of Technology, Electrical and Computer Engineering Department*, 2012.

[10] David Orbea, Jessica Moposita, Wilbert G Aguilar, Manolo Paredes, Rolando P Reyes, and Luis Montoya. Vertical take off and landing with fixed rotor. In *Proceedings of Conference on Electrical, Electronics Engineering, Information and Communication Technologies*, pages 1–6, Pucon, Chile, Oct. 2017. IEEE.

[11] Caitlin Powers, Daniel Mellinger, and Vijay Kumar. Quadrotor kinematics and dynamics. *Handbook of Unmanned Aerial Vehicles*, pages 307–328, 2015.

[12] Rached Dhaouadi and A Abu Hatab. Dynamic modelling of differential-drive mobile robots using Lagrange and Newton-Euler methodologies: A unified framework. *Advances in Robotics & Automation*, 2(2):1–7, 2013.

[13] Teppo Luukkonen. Modelling and control of quadcopter. *Independent Research Project in Applied Mathematics, Espoo*, 22, 2011.

[14] Jonathan How and Emilio Frazzoli. *16.30 Feedback Control Systems*. Massachusetts Institute of Technology: MIT OpenCourseWare, `https://ocw.mit.edu` License: Creative Commons BY-NC-SA., 2010.

[15] Chee Hwee Seah, Isonguyo J Inyang, and James F Whidborne. Bilinear modelling and attitude control of a quadrotor. *IFAC-PapersOnLine*, 50(2):193–198, 2017.

[16] Atheer L Salih, M Moghavvemi, Haider AF Mohamed, and Khalaf Sallom Gaeid. Flight PID controller design for a UAV quadrotor. *Scientific Research and Essays*, 5(23):3660–3667, 2010.

[17] Nizar Hadi Abbas and Ahmed Ramz Sami. Tuning of PID controllers for quadcopter system using hybrid memory based gravitational search algorithm–particle swarm optimization. *International Journal of Computer Applications*, 172(04):9–18, 2017.

[18] Saptarshi Das, Indranil Pan, and Shantanu Das. Multi-objective LQR with optimum weight selection to design FOPID controllers for delayed fractional order processes. *ISA transactions*, 58:35–49, 2015.

[19] Demet Canpolat Tosun, Y Isik, and Hakan Korul. Comparison of PID and LQR controllers on a quadrotor helicopter. *International Journal of Systems Applications, Engineering & Development*, 9:136–143, 2015.

[20] Rong Xu and Umit Ozguner. Sliding mode control of a quadrotor helicopter. In *Proceedings of the 45th IEEE Conference on Decision and Control*, pages 4957–4962, San Diego, CA, USA, Dec. 2006. IEEE.

[21] Tarek Madani and Abdelaziz Benallegue. Backstepping control for a quadrotor helicopter. In *Proceedings of IEEE/RSJ International Conference on Intelligent Robots and Systems*, pages 3255–3260, Beijing, China, Oct. 2006. IEEE.

[22] Yu Xu, Changfei Tong, and Huaizhong Li. Flight control of a quadrotor under model uncertainties. *International Journal of Micro Air Vehicles*, 7(1):1–19, 2015.

[23] Qi Lu, Beibei Ren, Siva Parameswaran, and Qing-Chang Zhong. Uncertainty and disturbance estimator-based robust trajectory tracking control for a quadrotor in

a global positioning system-denied environment. *Journal of Dynamic Systems, Measurement, and Control*, 140(3):031001, 2018.

[24] Ivana Palunko and Rafael Fierro. Adaptive control of a quadrotor with dynamic changes in the center of gravity. *IFAC Proceedings Volumes*, 44(1):2626–2631, 2011.

[25] Kunwu Zhang, Jicheng Chen, Yufang Chang, and Yang Shi. EKF-based LQR tracking control of a quadrotor helicopter subject to uncertainties. In *Proceedings of 42nd Annual Conference of the IEEE Industrial Electronics Society*, pages 5426–5431, Florence, Italy, Oct. 2016.

[26] Alejandro Astudillo, Bladimir Bacca, and Esteban Rosero. Optimal and robust controllers design for a smartphone-based quadrotor. In *Proceedings of IEEE 3rd Colombian Conference on Automatic Control*, pages 1–6, Cartagena, Colombia, Oct. 2017. IEEE.

[27] Prasanth Kotaru, Ryan Edmonson, and Koushil Sreenath. Geometric L_1 adaptive attitude control for a quadrotor unmanned aerial vehicle. *Journal of Dynamic Systems, Measurement, and Control*, 142(3), 2019.

[28] Jie Zhou, Ruiliang Deng, Zongying Shi, and Yisheng Zhong. Robust cascade PID attitude control of quadrotor helicopters subject to wind disturbance. In *Proceedings of 36th Chinese Control Conference*, pages 6558–6563, Dalian, China, Jul. 2017. IEEE.

[29] Moussa Labbadi and Mohamed Cherkaoui. Robust integral terminal sliding mode control for quadrotor UAV with external disturbances. *International Journal of Aerospace Engineering*, 2019.

[30] John C Doyle, Keith Glover, Pramod P Khargonekar, and Bruce A Francis. State-space solutions to standard H_2 and H_∞ control problems. *IEEE Transactions on Automatic Control*, 34(8):831–847, 1989.

[31] Keith Glover and John C Doyle. State-space formulae for all stabilizing controllers that satisfy an H_∞-norm bound and relations to relations to risk sensitivity. *Systems & Control Letters*, 11(3):167–172, 1988.

[32] Aleksandr Mikhailovich Lyapunov. The general problem of the stability of motion. *International Journal of Control*, 55(3):531–534, 1992.

[33] Mohammed Dahleh, Munther A Dahleh, and George Verghese. *6.241 Dynamic Systems and Control*. Massachusetts Institute of Technology: MIT OpenCourseWare, `https://ocw.mit.edu`, 2004.

[34] Jacobo Riccati. Animadversiones in aequationes differentiales secundi gradus. *Acta Eruditorum Lipsiae*, 1724.

[35] James Bellon. Riccati equations in optimal control theory. 2008.

[36] Saptarshi Das and Kaushik Halder. Missile attitude control via a hybrid LQG-LTR-LQI control scheme with optimum weight selection. In *Proceedings of First International Conference on Automation, Control, Energy and Systems*, pages 1–6, Hooghy, India, May. 2014. IEEE.

[37] Huibert Kwakernaak. H_2-optimization theory and applications to robust control design. *Annual Reviews in Control*, 26(1):45–56, 2002.

[38] KJ Hunt and V Kučera. The standard H_2-optimal control problem: a polynomial solution. *International Journal of Control*, 56(1):245–251, 1992.

[39] Kiyotsugu Takaba and Tohru Katayama. H_2 output feedback control for descriptor systems. *Automatica*, 34(7):841–850, 1998.

[40] Stephen Boyd, Laurent El Ghaoui, Eric Feron, and Venkataramanan Balakrishnan. *Linear Matrix Inequalities in System and Control Theory*, volume 15. SIAM, 1994.

[41] *Quanser UVS Multi-Vehicle Coordination User Manual*. Quanser Consulting Inc., Markham, Ontario, Canada, 2010.

[42] Michael S. Triantafyllou and Franz S. Hover. *2.154 Maneuvering and Control of Surface and Underwater Vehicles*. Massachusetts Institute of Technology: MIT OpenCourseWare, `https://ocw.mit.edu`, 2004.

[43] Mark W Spong and Mathukumalli Vidyasagar. *Robot Dynamics and Control*. John Wiley & Sons, 2008.

[44] Revaz V Gamkrelidze. Hamiltonian form of the maximum principle. *Control and Cybernetics*, 38(4A):959–971, 2009.

[45] Richard M Murray. *CDS112 Optimization-based Control*. California Institute of Technology, `http://www.cds.caltech.edu/~murray`, 2009.

[46] I-H Whang and S Cho. LQR gain-schedule controller for vertical line following. *Electronics Letters*, 46(14):991–993, 2010.

[47] Arthur Earl Bryson. *Control of Spacecraft and Aircraft*. Princeton university press Princeton, New Jersey, 1993.

[48] Richard M Murray. *CDS110 Analysis and Design of Feedback Systems*. California Institute of Technology, `http://www.cds.caltech.edu/~murray`, 2017.

[49] Hannu T Toivonen. Robust Control Methods. *Lecture Notes, Process Control Laboratory, Åbo Akademi University, Turku, Finland*, 1998.

[50] Tongwen Chen and Bruce A Francis. *Optimal Sampled-data Control Systems*. Springer Science and Business Media, 2012.

[51] Michael G Safonov, DJN Limebeer, and RY Chiang. Simplifying the H_∞ theory via loop-shifting, matrix-pencil and descriptor concepts. *International Journal of Control*, 50(6):2467–2488, 1989.

[52] Vladimir Kučera. A tutorial on H_2 control theory: The continuous time case. In *Polynomial Methods for Control Systems Design*, pages 1–55. Springer, 1996.

[53] Daria Madjidian. *Low-Rank Distributed Control with Application to Wind Energy*. Department of Automatic Control, Lund University, 2014.

[54] Alexandre Megretski. *6.245 Multivariable Control Systems*. Massachusetts Institute of Technology: MIT OpenCourseWare, `https://ocw.mit.edu`, 2004.

[55] Jonathan How. *16.323 Principles of Optimal Control*. Massachusetts Institute of Technology: MIT OpenCourseWare, `https://ocw.mit.edu`, 2008.

[56] Kemin Zhou, John Comstock Doyle, Keith Glover, et al. *Robust and Optimal Control*. Prentice hall New Jersey, 1996.

[57] Chi Tsong Chen. *Linear System Theory and Design*. Oxford University Press, Inc., 1995.

[58] Pascal Gahinet, Arkadii Nemirovskii, Alan J Laub, and Mahmoud Chilali. The LMI control toolbox. In *Proceedings of 33rd IEEE Conference on Decision and Control*, volume 3, pages 2038–2041, Lake Buena Vista, FL, USA, Dec. 1994. IEEE.

[59] Carsten Scherer, Pascal Gahinet, and Mahmoud Chilali. Multiobjective output-feedback control via LMI optimization. *IEEE Transactions on Automatic Control*, 42(7):896–911, 1997.

[60] Denis Arzelier. Course on LMI Optimization with Applications in Control. *LAAS-CNRS*, 2008.

[61] Robert E Skelton, Tetsuya Iwasaki, and Dimitri E Grigoriadis. *A Unified Algebraic Approach to Control Design*. CRC Press, 1997.

[62] Matthew M Peet. LMI Methods in Optimal and Robust Control. *Lecture Notes, Department of Mechanical and Aerospace Engineering, Arizona State University*, 2016.